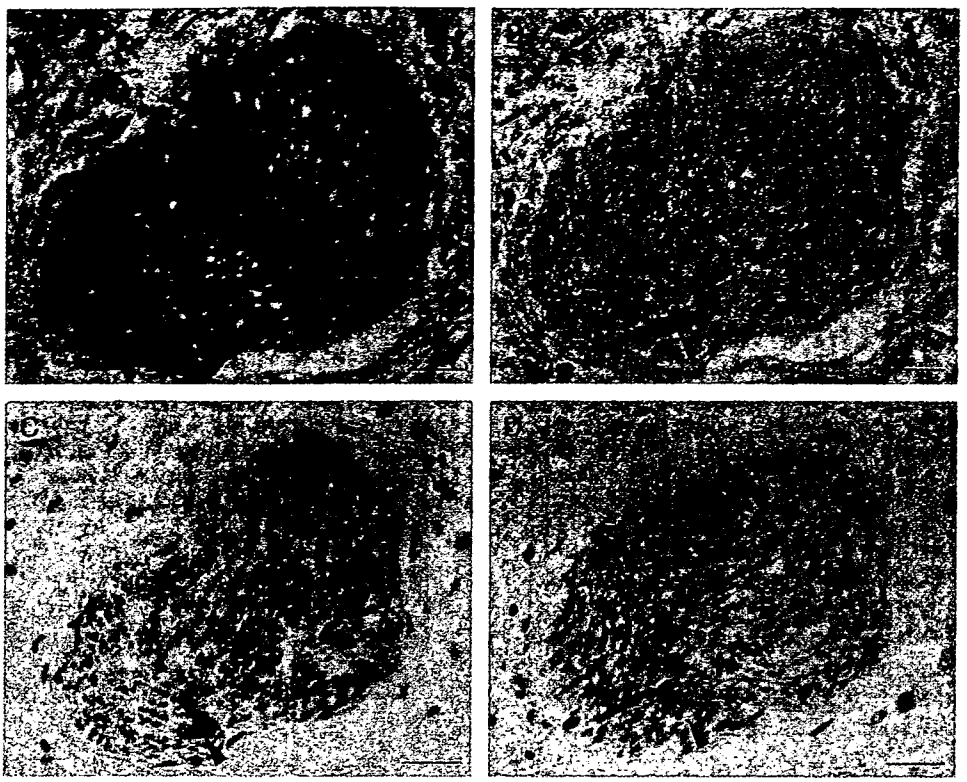

FIGURE 4. Lewy body-related α-synucleinopathy in a nerve fascicle from the fatty tissue surrounding the adrenal capsule. **(A)** An axonal pale body (arrowheads) is detectable with hematoxylin and eosin staining. **(B)** Anti-phosphorylated α-synuclein antibody (psyn#64) stains the pale body (arrowheads). Lewy dots are also visualized by the antibody. This image is a serial section of that shown in **(A)**. **(C)** Anti-tyrosine hydroxylase antibody clearly visualizes the pale body (arrowheads) as well as adjacent axons in the fascicle. This image is a serial section of that shown in **(B)**. **(D)** Anti-phosphorylated neurofilament antibody (SMI31) stains the periphery of the pale body (arrowheads) as well as axons of the nerve fascicle. This image is a serial section of that shown in **(C)**. Scale bars = **(A–D)** 25 μm.

all cases of PD. Because adrenal glands are routine sites of investigation in general autopsy, our results indicate that evaluation of the peripheral autonomic nervous system in Lewy body disease is possible through the examination of archival paraffin blocks of adrenal glands. Pathologic examination in TMGH requires strict removal of fatty tissue from adrenal glands to evaluate their exact weight. When such removal is not done, the detection rate of periadrenal paraganglia was almost 100% (Dr. K. Kawabata, Director, Department of Pathology, Akashi City Hospital, personal communication, 2006). Because the periadrenal retroperitoneal space contains abundant paraganglia and associated sympathetic ganglia and nerves, even the very thin surrounding tissue of the adrenal glands in our series always included useful peripheral sympathetic nervous tissue.

Adrenal glands are frequently affected by autolysis, inflammation, or metastasis, but our study suggests that the organs and the surrounding sympathetic ganglia and nerves are nevertheless useful for assessing morphologic changes in the peripheral autonomic nervous system in PD or DLB.

The amygdala variant of α-synucleinopathy is complicated by either a severe burden of tangles and plaques or by argyrophilic grains in the amygdala. This type of α-synucleinopathy is associated with AD and Down syndrome (25, 26, 43, 44), as well as with other tauopathies (45). We termed this type "secondary" (14, 15). The present study clearly shows that immunopathologic studies of the adrenal glands can distinguish secondary α-synucleinopathy from PD.

Braak et al (46) proposed a staging system for α-synucleinopathy in the brains of a nondemented general cohort and in cases of PD. Our series, with a cohort having a mean age of approximately 80 years, included a high percentage of dementia, as was expected. The differential diagnosis between DLB and PD with dementia is often difficult in such aged cohorts. Thus, Braak et al's staging paradigm could not be applied effectively to our group (15). We always examined the spinal cord, a structure not included in Braak et al's staging, to evaluate the preganglionic sympathetic neurons. Our results show that some DLB cases, whose α-synucleinopathy definitely involved sympathetic preganglionic neurons, did not present with α-synucleinopathy in the adrenal or periadrenal tissues. All of these cases met the morphologic criteria for AD from the elderly cohort (47) or for dementia with grains (28) and lacked a clinical description of parkinsonism. However, many other cases of DLB, complicated by similar changes in AD or dementia with grains and lacking a clinical description of parkinsonism, presented with α-synucleinopathy involving the adrenal or periadrenal tissues. Although

morphologic differences in the Lewy body pathology in the central nervous system at the final stage of the illness may become unclear, the pathologic examination of LBAS in the peripheral autonomic nervous system could delineate those DLB cases complicated by other senile changes and presenting with a limbic-neocortical-dominant distribution of Lewy body pathology, lesser involvement of the brainstem and spinal cord, and a lack of adrenal and periadrenal Lewy body pathology from other DLB cases with a pathology more common to PD (with or without dementia), which always presents with adrenal or periadrenal Lewy body pathology.

Although the number of cases was small, 2 cases presented with Lewy bodies only in the adrenal glands and lacked Lewy bodies in the central nervous system. These cases could possibly represent the earliest stage of Lewy body-related progressive autonomic failure. From the points of disease pathogenesis and hierarchy of the Lewy body disorders, this result indicates that the adrenal gland could be the initial and primary target for these progressive disorders.

In the present study, we retrospectively investigated the correlation between clinical and pathologic presentations of adrenal glands. Although there were definite limitations in our study based on the review of medical records, the observed Lewy body-related pathology involving adrenal tissues did not correspond to any symptomatology of adrenal insufficiency, except for orthostatic hypotension. Also, our studies did not indicate how to detect this adrenal or periadrenal Lewy body-related pathology in clinical testing. Reduced uptake of MIBG in cardiac scintigraphy in Lewy body disease corresponds to decreased TH-immunoreactivity as well as to α-synucleinopathy in unmyelinated fibers from the epicardial fatty tissue of the anterior wall of the left ventricle of the heart (8–10). However, because the TH-immunoreactive unmyelinated fibers in the periadrenal fatty tissue were relatively preserved in this study, MIBG scintigraphy, which is also used for the detection of pheochromocytoma of the adrenal glands, may not be useful for detection of this Lewy body-related pathology in adrenal tissues. Therefore, we are now planning a prospective functional study of cases with Lewy body disease consisting of the tilt test and simultaneous blood sampling to gauge the serum noradrenalin level, as well as the resting adrenalin level, to detect this adrenal pathology clinically.

In conclusion, the immunohistochemical examination of adrenal glands with anti-phosphorylated α-synuclein antibodies can help differentiate the primary and the secondary forms of LBAS, as well as identify where LBAS starts in the human body and how it spreads.

ACKNOWLEDGMENTS

We thank Mr. Naoo Aikyo, Ms. Mieko Harada, and Ms. Nobuko Naoi (Department of Neuropathology, Tokyo Metropolitan Institute for Gerontology) for the preparation of sections and Dr. Kinuko Suzuki (Department of Pathology and Laboratory Medicine, University of North Carolina at Chapel Hill) for helpful discussions. We also thank two anonymous neurologists for preparing the Clinical Dementia Rating scores used in this study.

REFERENCES

1. Kosaka K. Dementia and neuropathology in Lewy body disease. Adv Neurol 1993;60:456–63
2. Kosaka K, Yoshimura M, Ikeda K, Budka H. Diffuse type of Lewy body disease: Progressive dementia with abundant cortical Lewy bodies and senile changes of varying degree-a new disease? Clin Neuropathol 1984;3:185–92
3. Koike Y, Takahashi A. Autonomic dysfunction in Parkinson's disease. Eur Neurol 1997;38(Suppl 2):8–12
4. Horimoto Y, Matsumoto M, Akatsu H, et al. Autonomic dysfunctions in dementia with Lewy bodies. J Neurol 2003;250:530–33
5. Hishikawa N, Hashizume Y, Yoshida M, Sobue G. Clinical and neuropathological correlates of Lewy body disease. Acta Neuropathol (Berl) 2003;105:341–50
6. Hakusui S, Yasuda T, Yanagi T, et al. A radiological analysis of heart sympathetic functions with meta-[^{123}I]iodobenzylguanidine in neurological patients with autonomic failure. J Auton Nerv Syst 1994;49: 81–84
7. Orimo S, Ozawa E, Nakade S, Sugimoto T, Mizusawa H. (^{123})I-metaiodobenzylguanidine myocardial scintigraphy in Parkinson's disease. J Neurol Neurosurg Psychiatry 1999;67:189–94
8. Orimo S, Oka T, Miura H, et al. Sympathetic cardiac denervation in Parkinson's disease and pure autonomic failure but not in multiple system atrophy. J Neurol Neurosurg Psychiatry 2002;73:776–77
9. Orimo S, Amino T, Takahashi A, et al. Cardiac sympathetic denervation in Lewy body disease. Parkinsonism Relat Disord 2006; 12:S99–105
10. Mitsui J, Saito Y, Momose T, et al. Pathology of the sympathetic nervous system corresponding to the decreased cardiac uptake in ^{123}I-metaiodobenzylguanidine (MIBG) scintigraphy in a patient with Parkinson disease. J Neurol Sci 2006;243:101–4
11. Yoshita M, Taki J, Yokoyama K, et al. Value of ^{123}I-MIBG radioactivity in the differential diagnosis of DLB from AD. Neurology 2006; 66:1850–54
12. Forno LS, Sternberger LA, Sternberger NH, Strefling AM, Swanson K, Eng LF. Reaction of Lewy bodies with antibodies to phosphorylated and non-phosphorylated neurofilaments. Neurosci Lett 1986;64:253–58
13. Wakabayashi K, Takahashi H. Neuropathology of autonomic nervous system in Parkinson's disease. Eur Neurol 1997;38(Suppl 2):2–7
14. Saito Y, Kawashima A, Ruberu NN, et al. Accumulation of phosphorylated α-synuclein in aging human brain. J Neuropathol Exp Neurol 2003;62:644–54
15. Saito Y, Ruberu NN, Sawabe M, et al. Lewy body-related α-synucleinopathy in aging. J Neuropathol Exp Neurol 2004;63:742–49
16. Yamaguchi H, Haga C, Hirai S, Nakazato Y, Kosaka K. Distinctive, rapid, and easy labeling of diffuse plaques in the Alzheimer brains by a new methenamine silver stain. Acta Neuropathol 1990;79:569–72
17. Gallyas F. Silver staining of Alzheimer's neurofibrillary changes by means of physical development. Acta Morphol Acad Sci Hung 1971; 19:1–8
18. Saito Y, Nakahara K, Yamanouchi H, Murayama S. Severe involvement of ambient gyrus in dementia with grains. J Neuropathol Exp Neurol 2002;61:789–96
19. Fujiwara H, Hasegawa M, Dohmae N, et al. α-Synuclein is phosphorylated in synucleinopathy lesions. Nat Cell Biol 2002;4:160–64
20. Jakes R, Crowther RA, Lee VM, Trojanowski JQ, Iwatsubo T, Goedert M. Epitope mapping of LB509, a monoclonal antibody directed against human α-synuclein. Neurosci Lett 1999;269:13–16
21. McKeith IG, Galasko D, Kosaka K, et al. Consensus guidelines for the clinical and pathologic diagnosis of dementia with Lewy bodies (DLB): Report of the consortium on DLB international workshop. Neurology 1996;47:1113–24
22. McKeith IG, Dickson DW, Lowe J, et al. Diagnosis and management of dementia with Lewy bodies: Third report of the DLB Consortium. Neurology 2005;65:1863–72
23. Dickson DW, Schmidt ML, Lee VM, Zhao ML, Yen SH, Trojanowski JQ. Immunoreactivity profile of hippocampal CA2/3 neurites in diffuse Lewy body disease. Acta Neuropathol (Berl) 1994;87:269–76

24. Forman MS, Schmidt ML, Kasturi S, Perl DP, Lee VM, Trojanowski JQ. Tau and α-synuclein pathology in amygdala of Parkinsonism-dementia complex patients of Guam. Am J Pathol 2002;160:1725–31
25. Uchikado H, Lin WL, DeLucia MW, Dickson DW. Alzheimer disease with amygdala Lewy bodies: A distinct form of α-synucleinopathy. J Neuropathol Exp Neurol 2006;65:685–97
26. Hamilton RL. Lewy bodies in Alzheimer's disease: A neuropathological review of 145 cases using α-synuclein immunohistochemistry. Brain Pathol 2000;10:378–84
27. Braak H, Braak E. Neuropathological staging of Alzheimer-related changes. Acta Neuropathol 1991;82:239–59
28. Saito Y, Ruberu NN, Sawabe M, et al. Staging of argyrophilic grains: An age-associated tauopathy. J Neuropathol Exp Neurol 2004; 63:911–18
29. Murayama S, Saito Y. Neuropathological diagnostic criteria for Alzheimer's disease. Neuropathology 2004;24:254–60
30. Jellinger KA. Dementia with grains (argyrophilic grain disease). Brain Pathol 1998;8:377–86
31. Jellinger KA, Bancher C. Senile dementia with tangles (tangle predominant form of senile dementia). Brain Pathol 1998;8:367–76
32. Roman GC, Tatemichi TK, Erkinjuntti T, et al. Vascular dementia: Diagnostic criteria for research studies. Report of the NINDS-AIREN International Workshop. Neurology 1993;43:250–60
33. Hauw JJ, Daniel SE, Dickson D, et al. Preliminary NINDS neuropathologic criteria for Steele-Richardson-Olszewski syndrome (progressive supranuclear palsy). Neurology 1994;44:2015–19
34. Folstein MF, Folstein SE, McHugh PR. "Mini-mental state": A practical method for grading the cognitive state of patients for the clinician. J Psychiatr Res 1975;12:189–98
35. Hasegawa K, Inoue K, Moriya K. An investigation of dementia rating scale for the elderly (in Japanese). Seishin Igaku 1974;16:965–69
36. Katoh S, Simogaki H, Onodera A, et al. Development of the revised version of Hasegawa's dementia scale (HDS-R). Rounen Seishinigaku Zashi 1991;2:1339–47
37. Lawton MP, Brody EM. Assessment of older people: self-maintaining and instrumental activities of daily living. Gerontologist 1969;9:179–86
38. Hughes CP, Berg L, Danziger WL, Coben LA, Martin RL. A new clinical scale for the staging of dementia. Br J Psychiatry 1982;140: 566–72
39. Mahoney FI, Barthel DW. Functional evaluation: The Barthel Index. Md State Med J 1965;14:61–65
40. Kimula Y, Utsuyama M, Yoshimura M, Tomonaga M. Element analysis of Lewy and adrenal bodies in Parkinson's disease by electron probe microanalysis. Acta Neuropathol (Berl) 1983;59:233–36
41. Wakabayashi K, Takahashi H, Ohama E, Takeda S, Ikuta F. Lewy bodies in the visceral autonomic nervous system in Parkinson's disease. Adv Neurol 1993;60:609–12
42. Forno LS, Norville RL. Ultrastructure of Lewy bodies in the stellate ganglion. Acta Neuropathol (Berl) 1976;34:183–97
43. Lippa CF, Fujiwara H, Mann DM, et al. Lewy bodies contain altered α-synuclein in brains of many familial Alzheimer's disease patients with mutations in presenilin and amyloid precursor protein genes. Am J Pathol 1998;153:1365–70
44. Lippa CF, Schmidt ML, Lee VM, Trojanowski JQ. Antibodies to α-synuclein detect Lewy bodies in many Down's syndrome brains with Alzheimer's disease. Ann Neurol 1999;45:353–57
45. Yamazaki M, Arai Y, Baba M, et al. α-Synuclein inclusions in amygdala in the brains of patients with the parkinsonism-dementia complex of Guam. J Neuropathol Exp Neurol 2000;59:585–91
46. Braak H, Del Tredici K, Rub U, de Vos RA, Jansen Steur EN, Braak E. Staging of brain pathology related to sporadic Parkinson's disease. Neurobiol Aging 2003;24:197–211
47. Knopman DS, Parisi JE, Salviati A, et al. Neuropathology of cognitively normal elderly. J Neuropathol Exp Neurol 2003;62:1087–95

Granular Tau Oligomers as Intermediates of Tau Filaments†

Sumihiro Maeda,‡ Naruhiko Sahara,‡ Yuko Saito,§ Miyuki Murayama,‡ Yuji Yoshiike,‡ Hyonchol Kim,‖,⊥ Tomohiro Miyasaka,‡ Shigeo Murayama,§ Atsushi Ikai,‖ and Akihiko Takashima*,‡

Lab for Alzheimer's Disease, RIKEN Brain Science Institute, 2-1 Hirosawa, Wako, Saitama 351-0198, Japan, Department of Neuropathology and Department of Pathology, Tokyo Metropolitan Institute of Gerontology, Tokyo Metropolitan Geriatric Hospital, 35-2 Sakaecho, Itabashi-ku, Tokyo 173-0015, Japan, and Department of Life Science, Graduate School of Bioscience and Biotechnology, Tokyo Institute of Technology, 4259 Nagatsuda, Midori-ku, Yokohama, Kanagawa 226-8501, Japan

Received July 6, 2006; Revised Manuscript Received December 15, 2006

ABSTRACT: Neurofibrillary tangles (NFTs) are pathological hallmarks of several neurodegenerative disorders, including Alzheimer's disease (AD). NFTs are composed of microtubule-binding protein tau, which assembles to form paired helical filaments (PHFs) and straight filaments. Here we show by atomic force microscopy that AD brain tissue and in vitro tau form granular and fibrillar tau aggregates. CD spectral analysis and immunostaining with conformation-dependent antibodies indicated that tau may undergo conformational changes during fibril formation. Enriched granules generated filaments, suggesting that granular tau aggregates may be an intermediate form of tau fibrils. The amount of granular tau aggregates was elevated in prefrontal cortex of Braak stage I cases compared to that of Braak stage 0 cases, suggesting that granular tau aggregation precedes PHF formation. Thus, granular tau aggregates may be a relevant marker for the early diagnosis of tauopathy. Reducing the level of these aggregates may be a promising therapy for tauopathies and for promoting healthy brain aging.

Neurofibrillary tangles (NFTs)[1] are common in many neurodegenerative diseases and to some degree in normal aging (*1*, *2*). NFTs are intracellular neuronal clusters of fibrils that consist of paired helical filaments (PHFs) and straight filaments (SFs). These filaments are composed of hyperphosphorylated tau, a type of microtubule-binding protein. Some have proposed a connection between NFT formation and neuronal loss, because NFTs are observed in brain regions that also exhibit neuronal loss (*3*). Recent genetic studies of frontotemporal dementia with parkinsonism linked to chromosome 17 (FTDP-17) revealed that a mutation in the tau gene induces NFT formation and neuronal loss (*4*), suggesting that tau dysfunction itself could lead to NFT formation and neuronal loss.

It is unclear, however, how tau forms fibrils and how tau contributes to neurodegeneration. A recent report showed that inhibiting tau expression in tau transgenic mice protected against neuronal death, even though NFTs were still produced (*5*). These results suggest that the degenerating pathway, triggered by tau overexpression, may branch from a tau filament formation pathway. Tau may produce toxic aggregates before forming tau fibrils.

Tau fibril formation has been studied extensively in vitro. Anionic surfactants accelerate fibril formation of tau protein in vitro (*6*). Fibril formation can be monitored by thioflavin fluorescence, which recognizes aggregations having a β-sheet conformation. In this study, together with the thioflavin assay, we applied atomic force microscopy (AFM) to tau in solution to track structural changes in tau and to identify intermediates of tau filaments.

MATERIALS AND METHODS

Expression and Purification of Recombinant Tau Protein. Recombinant human tau (2N4R) in the pRK172 vector was purified using methods described previously (*7*) with some modifications. Details of these methods are described in the Supporting Information. After being freeze-dried, tau was dissolved in water and stored as a stock solution at −30 °C.

Incubation of Tau and Fluorescence Spectroscopy (ThT assay). The degree of tau aggregation was determined using thioflavin T (ThT) (*8*). Tau or BSA (control protein) stock solutions were diluted to 10 μM with 10 mM HEPES (pH 7.4), 100 mM NaCl, 10 μM heparin, and 10 μM ThT (final volume of 50 μL per well) and incubated in a damp box at 37 °C. At indicated time points (see Figure 2), we measured ThT fluorescence levels as previously described (*9*).

Atomic Force Microscopy (AFM). A multimode Nanoscope IIIa (Digital Instruments, Santa Barbara, CA) equipped

† This work is partly supported by a Grant-in-Aid for Scientific Research (11680746, from the Japanese Ministry of Education, Science, and Culture) and Promotion of Novel Interdisciplinary Fields Based on Nanotechnology and Materials.

* To whom correspondence should be addressed. E-mail: kenneth@brain.riken.jp. Telephone: +81-(0)48-467-9627. Fax: +81-(0)48-467-5916.

‡ RIKEN Brain Science Institute.

§ Tokyo Metropolitan Geriatric Hospital.

‖ Tokyo Institute of Technology.

⊥ Present address: Department of Biomedical Information, Division of Biosystems, Institute of Biomaterials and Bioengineering, Tokyo Medical and Dental University, 2-3-10 Surugadai, Chiyoda-ku, Tokyo 101-0062, Japan.

[1] Abbreviations: NFT, neurofibrillary tangle; PHF, paired helical filament; SF, straight filament; FTDP-17, frontotemporal dementia with parkinsonism linked to chromosome 17; AFM, atomic force microscopy; dLLS, dynamic laser light scattering; sLLS, static laser light scattering; CD, circular dichroism; ThT, thioflavin T; BSA, bovine serum albumin.

10.1021/bi061359o CCC: $37.00
Published on Web 03/06/2007

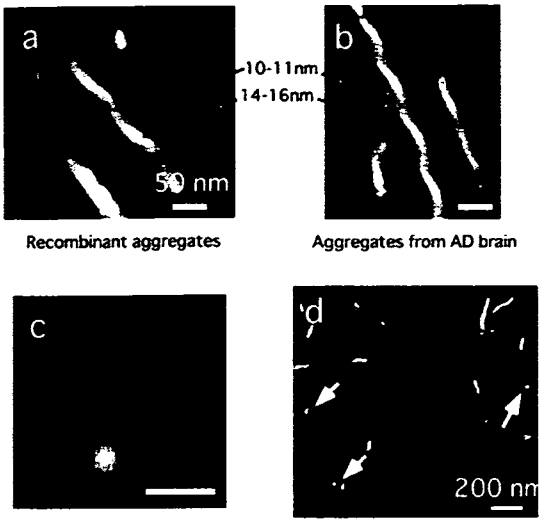

FIGURE 1: AFM images of recombinant tau aggregates in solution, fibrils (a) and granules (c). AFM images of PHFs and straight filaments purified from an AD brain (b). The heights of "mountains and valleys" of the twisted filaments are indicated. Tau-enriched fractions from the AD brain contain tau fibrils and granules (arrow) (d). Scale bars are 50 (a–c) and 200 nm (d).

with tapping mode was used for AFM observations in solution. An OMCL-TR400PSA device (Olympus) was used as a microcantilever. Incubated tau solutions from three different Black Cliniplate wells were combined, dropped onto freshly cleaved mica, allowed to set for 10 min, and then examined via AFM. For human tau, samples were left on the mica surface for 30 min and washed once with buffer prior to AFM assessment. We processed the height images of structures using NIH-image 1.62 and calculated the major (length) and minor (diameter) axes for each particle. Data from four different regions (4 μm^2) of each structure were plotted.

Sucrose Step Gradients and Preparation of Concentrated Tau. An incubated or immunoaffinity-purified tau solution (1 mL) was fractionated using discontinuous sucrose gradients using a TLA 55 rotor (Beckman) on a 5 mL scale as described previously (*10*). To concentrate the fractions and for buffer exchanges with 10 mM HEPES and 100 mM NaCl, we filtered the fractions using Centricut mini filters (10 kDa cutoff; KURABOU) at room temperature for 1 or 2 days. Although granular tau oligomers are insoluble in sarcosyl (Figure 1 of the Supporting Information), most remained in the supernatant fraction after ultracentrifugation (100K*g* for 30 min) because of their small sedimentation coefficient. Centrifuging the supernatant fraction at 200K*g* for 2 h, however, successfully separated the oligomers from soluble and flexible tau species.

Dot Blot Analysis. The tau protein concentration in each fraction was determined using amino acid hydrolysis, and the same amount of tau was dotted onto nitrocellulose membranes. We used the following primary antibodies: E1 (recognizes total tau), MC1 (recognizes PHF tau conformational change; generous gift from P. Davies, Albert Einstein College of Medicine, Bronx, NY), and A11 (recognizes the conformation of toxic Aβ; Biosource) (*11*). The membranes were incubated with peroxidase-labeled secondary antibody and visualized using ECL.

Laser Light Scattering and Circular Dichroism Spectroscopy. The buffers from fractions 1 and 3 were exchanged with high-salt buffer [10 mM Tris (pH 7.4) and 800 mM NaCl] to minimize further aggregation. To ensure the elimination of filaments formed in the filtering step, the sample was centrifuged at 100K*g* for 30 min at 4 °C. After we had confirmed that the granular aggregates were not filamentous using AFM, the tau oligomeric fraction was subjected to static and dynamic laser light scattering using a Zetasizer (Sysmex) at 23 °C. The molecular mass of granular tau oligomer was calculated as the average of triplicate experiments.

We measured the circular dichroism (CD) spectra of each fraction with a J-720 spectropolarimeter (Jasco). Samples placed in a cuvette with a path length of 1 mm were measured from 200 to 260 nm at 23 °C. Spectra obtained from an average of 20 scans were converted to mean residue ellipticity.

Human Brain Sample Preparation. Granular tau oligomer fractions from human brains were purified according to procedures described previously (*10*). Significant differences between each Braak stage were tested with the Kruskal Wallis test. Data were analyzed with InStat 3 for Macintosh (Graphpad, San Diego, CA).

RESULTS

Assessing the Formation of Filaments and Granules by AFM. AFM examination of a tau solution incubated for 72 h revealed the presence of twisted filaments (Figure 1a) resembling PHFs (Figure 1b). This experimental system allowed us to observe both filament and granule formation (Figure 1a,c). AFM examination of immunoaffinity-purified tau from AD brains revealed granules that are the same size as those observed in the in vitro tau aggregation system (Figure 1d). Granules and tau filaments were insoluble in *N*-lauroylsarcosine (sarcosyl) detergent (Figure 1 of the Supporting Information). These observations suggest that tau aggregates may form two different structures, granules and fibrils, both in vitro and in vivo.

Granule Formation Precedes Filament Formation. To understand the relationship between these different tau aggregates, we investigated how tau assembly in vitro changes over time by measuring ThT fluorescence and by using AFM. During the first incubation period of 4 h, ThT fluorescence levels remained constant and no aggregates were observed via AFM (Figure 2a of the Supporting Information). After incubation for 4 h, however, ThT fluorescence levels increased and spherically or elliptically shaped granules and fibrils formed (Figure 2a,b of the Supporting Information). We used the major-to-minor axis ratio to define granules ($1 \leq$ major-to-minor axis ratio < 2) and fibrils ($2 \leq$ major-to-minor axis ratio) and then determined temporal changes in ThT fluorescence (Figure 2). At incubation for 6 h, granule levels increased rapidly, reaching a plateau at 21 h. After incubation for 21 h, even though the levels of granular tau oligomers had plateaued, tau fibrils continued to grow. The number and length of fibrils continued to increase with incubation times of up to 328 h, reaching lengths of up to 950 nm and diameters of 15–25 nm (Figure 2c of the Supporting Information).

ThT fluorescence intensity seemed to correspond to both granular and fibrillar tau levels, suggesting that both granules

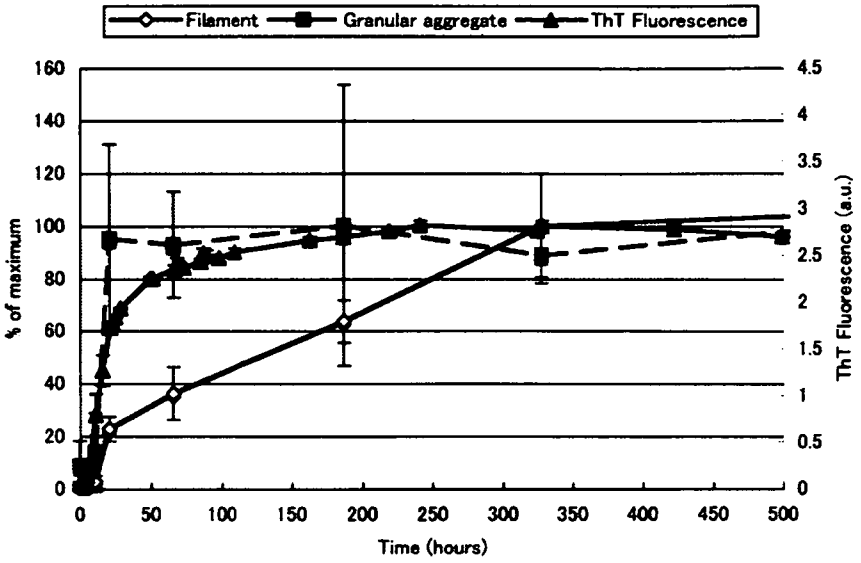

FIGURE 2: Temporal changes in ThT fluorescence and in granular tau oligomer and tau fibril levels. The ThT fluorescence of tau aggregation was measured at the indicated time points (mean ± standard deviation; $n = 3$). Tau granule and fibril levels were determined by calculating the area occupied from AFM images of tau samples taken at each time point (Figure 2b,c of the Supporting Information). Data are represented as percentages of the maximum oligomer and fibril levels (mean ± standard deviation).

and fibrils may possess a β-sheet conformation. These results led us to conclude that the granular tau oligomer might represent an intermediate form of tau fibril.

Characterization of Granular Tau Aggregates. We characterized granular tau aggregates by separating granular tau oligomers from the tau aggregate mixture. We then fractionated the incubated sample using sucrose gradient ultracentrifugation (Figure 3a). While fraction 1 contained no apparent aggregate, fraction 3 contained the largest amounts of granular tau oligomers. The size of granules in fraction 3 was normally distributed, with the largest sizes reaching 15−25 nm, as determined by AFM. Fractions 4−6 contained filaments. Since we could not assess by AFM the contamination of fraction 3 with soluble tau, we employed dynamic laser light scattering (dLLS) to assess soluble tau. dLLS analysis of fraction 3 revealed a single-peak distribution distinct from that of soluble tau (Figure 3b). Therefore, we concluded that fraction 3 does not contain fibrils or soluble tau but instead contains granular tau aggregates.

The temporal change of tau levels in each fraction was investigated using CBB staining after electrophoresis. In fraction 1 (soluble tau fraction), the amount of tau was reduced, corresponding to an increasing level of granular tau oligomer and fibril formation; tau levels in fraction 3 (granular tau oligomer fraction) decreased at later stages of the incubation, while the tau level in fraction 6 (filament fraction) continuously increased (Figure 3 of the Supporting Information). This result supports the observation under AFM that granular tau oligomer may be an intermediate form for tau filament.

We used fraction 3 to determine an approximate molecular mass of the granular tau oligomer. Figure 3c shows a Debye plot obtained from static laser light scattering (sLLS) analysis of granular oligomeric tau. The KC/RoP value at the y-intercept (sample concentration of zero) equals the reciprocal of the approximate molecular mass of the granular tau oligomer (Figure 3c). The approximate molecular mass of the granular tau oligomer averaged 1843.3 ± 112.4 kDa (average ± standard deviation; $n = 3$ replications), corresponding to 40 ± 3 tau molecules. KC/RoP values decreased as the sample concentration increased; that is, the granular tau oligomer has a negative second virial coefficient indicative of adhesive properties (*12*).

Conformational Differences between Granular and Fibrillar Tau. We used circular dichroism (CD) spectral analysis to analyze structural differences between soluble (fraction 1), granular oligomeric (fraction 3), and fibrillar forms (pellet, fraction 6) of tau. The spectral curve of fraction 1 had a minimum ellipticity of approximately 200 nm, indicating a random coil structure (*13*). Fibrillar tau (fraction 6) had fewer random coil structures and a growing "shoulder" in the curve at ~220 nm, indicating β-sheet structure. The CD spectrum of the granular tau oligomer (fraction 3) also revealed a shoulder smaller than that of fibrillar tau at ~220 nm (Figure 3d). The CD spectrum of granular tau oligomers was distinct but intermediate in form compared to those of soluble and fibrillar tau, suggesting that the granular tau oligomer may represent an intermediate structure. This observation was confirmed by probing samples of each tau fraction with conformation-dependent antibodies (Figure 3e). E1 antibody, which recognizes the N-terminus of tau, immunostained all fractions to the same extent. MC1, which recognizes a conformational change in PHF, did not immunostain the soluble tau fraction (fraction 1) but did immunostain granular and fibrillar tau fractions (fractions 2−6). A11 antibody, which recognizes toxic oligomers of β-amyloid, immunostained only fibrillar fractions (fractions 4−6). Taken together, these results indicate that tau fibrils might have another conformational form having an additional structure distinct from that of granular tau oligomer.

Conversion of Granular Aggregates into Filaments. To examine whether granular tau aggregates could form filaments, we enriched the concentration of tau by filtering fractions 1 and 3. Samples containing enriched granular tau oligomer formed filaments (Figure 4c,d), while samples containing enriched soluble tau failed to form aggregates

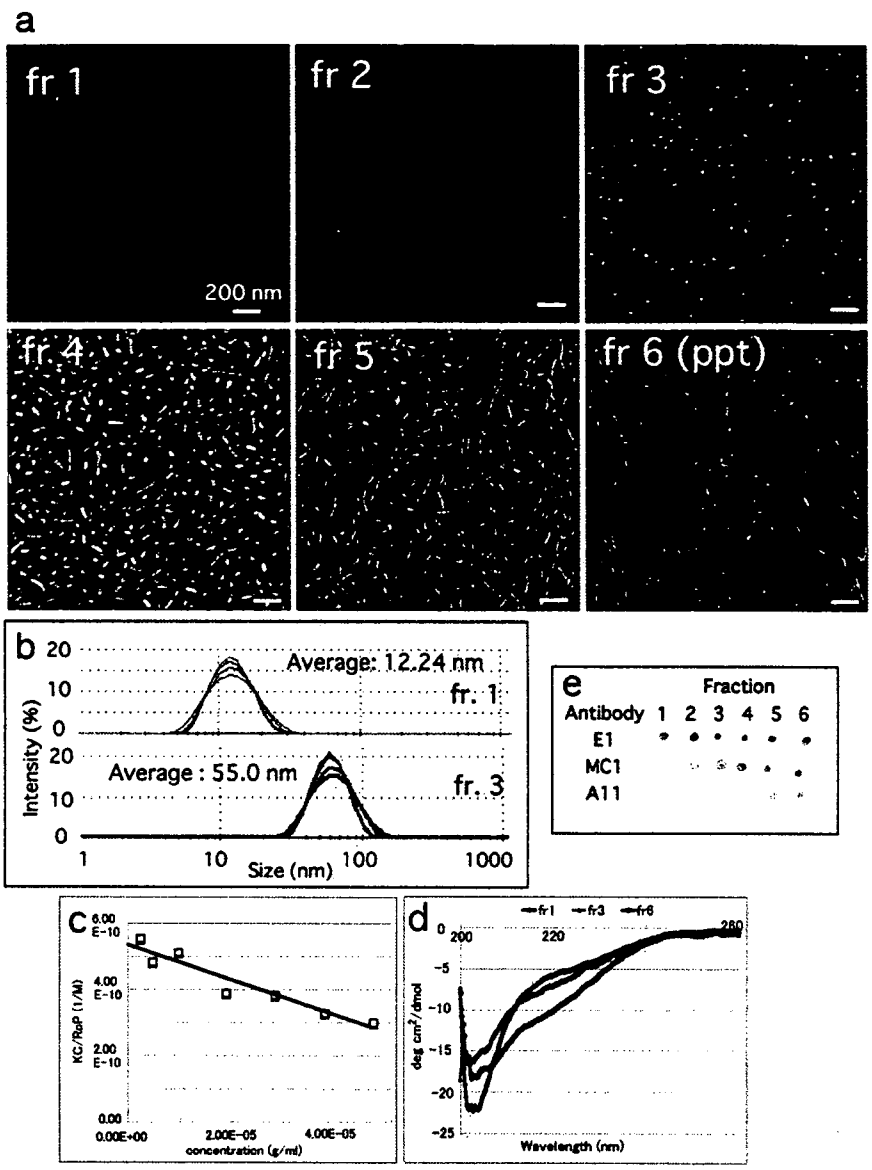

FIGURE 3: Purification and characterization of granular tau oligomers. (a) AFM images of fractions after sucrose gradient centrifugation. The scale bar is 200 nm. (b) Size distribution of soluble tau (fraction 1) and granular tau (fraction 3) as determined by dynamic laser light scattering. Fraction 1 displayed a distribution similar to that of monomeric tau species. Fraction 3, however, displayed a distribution of structures distinct from that of fraction 1, indicating that nonaggregated tau species do not contaminate fraction 3. (c) Analysis of the granular tau oligomer fraction using static laser light scattering. Debye plot of KC/RoP for different tau concentrations (□). The y-intercept value of the best linear fit indicates the approximate reciprocal of the molecular mass of granular oligomeric tau. (d) CD spectrum of fractions 1 (soluble tau oligomer), 3 (granular tau oligomer), and 6 (tau fibril). (e) The same amount of tau in each fraction was dotted onto nitrocellulose membranes and probed with the indicated antibodies.

(Figure 4a,b). These results strongly suggest that tau fibrils stem from granular tau oligomers or, in other words, that the granular tau oligomer is an intermediate form of tau fibril.

To confirm that granular tau aggregates form before the formation of tau fibrils in vivo, we purified, by immunoaffinity purification and sucrose gradient centrifugation, granular tau aggregates from human frontal cortex of cases evaluated to be at different Braak stages. As with the recombinant tau aggregation experiment, we detected granular tau oligomers in fraction 3 (Figure 4 of the Supporting Information) derived from Braak stage V samples (which have NFTs) (Figure 4e). Then, we could also detect them in fraction 3 derived from Braak stage 0 samples (which have no NFTs) (Figure 4e). The amount of granules in the Braak stage 0 samples, however, was significantly low. We also examined PHF-tau in Braak stage 0, I, III, and V samples by using a precipitation method (*14*) and found high levels of PHF-tau in Braak stage V brains but no detectable levels of PHF-tau in Braak stage 0, I, and III brains (*10*). These observations are consistent with the pathological evaluations of these brains.

Quantitative analysis showed increased levels of granular tau even in samples at Braak stage I, a stage characterized by the lack of NFTs in the frontal cortex. This finding suggests that tau granules accumulate far before tau fibrils form. Similar to what we found in our in vitro tau aggregation

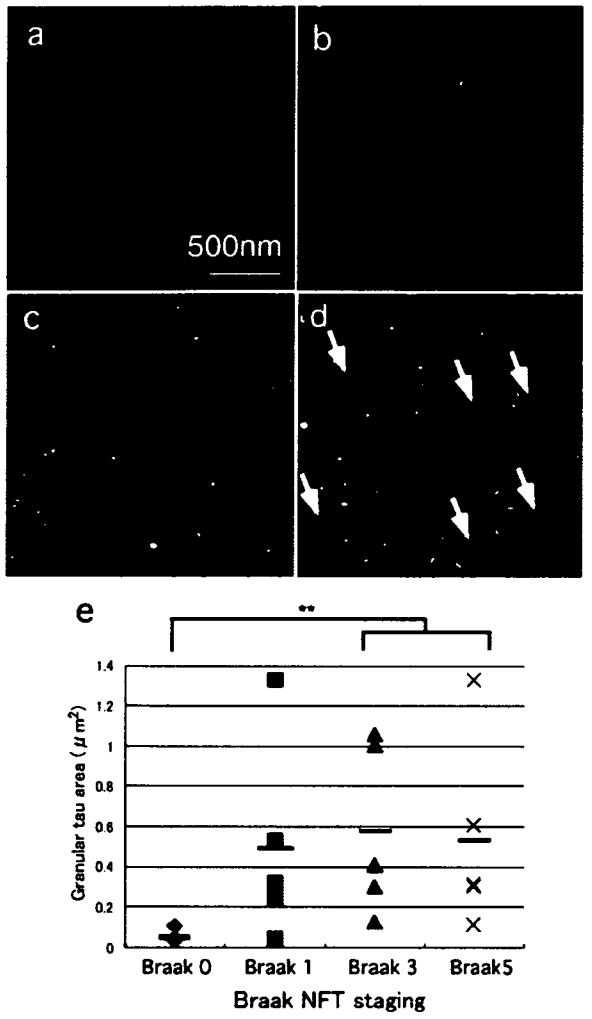

FIGURE 4: Tau filaments generated from granular tau oligomers. (a–d) AFM images of fractions 1 (a and b) and 3 (c and d), before (a and c) and after (b and d) the samples had been concentrated in the absence of heparin. Although concentrated fraction 1 had no structures, concentrated fraction 3 generated filaments (arrows). (e) The granular tau oligomer was purified as described in Materials and Methods from pathologically staged frontal cortex samples. Quantitative measurements of tau present in fraction 3 were derived from NIH-image 1.62 and are represented as the area (square micrometers) occupied by tau granules Two asterisks denote $p = 0.0155$ (Kruskal Wallis test).

experiments, high concentrations of granular tau oligomers in vivo may also lead to tau fibril formation in the brains of individuals with AD. Thus, granular tau oligomers may also represent an intermediate structure of tau during tau fibril formation in the human brain.

DISCUSSION

Tau Filaments Develop from Granular Tau Oligomers. Here we report that 40mer tau oligomers form granular structures having an MC1 epitope, indicating that this granular tau oligomer consists of conformationally changed tau. Partially folded tau monomers that are distinct from native tau monomers and that display a reduced level of random coiling but an increased level of β-sheet conformation have been reported previously (*15*). This type of conformation is similar to that displayed by granular tau oligomers; therefore, granular oligomers may be composed of these monomers.

Fibrils have a tendency to take on β-sheet conformations and also stain positively for anti-oligomer A11 antibody (*11*), which is consistent with our finding that A11 specifically recognizes proteins having either β-barrel or β-sandwich structures (Y. Yoshiike and A. Takashima, unpublished data). Therefore, tau fibrils may be composed of an assembly of granular tau aggregates having a β-sheet structure. Smaller granules of tau oligomers may grow by binding with soluble tau. Once the oligomer reaches a size of 20 nm, binding of granular tau oligomers enables tau fibrils to develop. This premise is consistent with our observation that only granular tau oligomers were detectable in the early stages of incubation, and the fact that fibrils appeared after longer incubations and CBB staining after electrophoresis in each fraction also support this idea (Figure 3 of the Supporting Information). After incubation for 7 months (5500 h), all tau monomers and granular tau oligomers had converted into filaments (data not shown). These observations are consistent with our hypothesis that the granular tau oligomer represents an intermediate form of tau filament.

In prions, complex pathways determine whether monomers derived from dissociated oligomers convert into filaments (*16*). Using our recombinant tau aggregation system, we examined fraction 3 to determine whether tau oligomers dissociate to form monomers, but we found no monomer contamination in fraction 3 (Figure 3b). After concentrating soluble tau and granular tau fractions (fractions 1 and 3, respectively), we found that granular tau, not soluble tau, is capable of forming filaments without additional heparin. This indicated that granular tau represents an intermediate form but that soluble tau does not. The mechanism underlying filament elongation by binding of granular tau oligomer needs further clarification.

Granular Tau Oligomers in Human Brain. Granular tau oligomers have been found in human brains. These oligomers consist of highly phosphorylated tau and are similar in size to granular tau oligomers derived from recombinant tau (*10*). PHFs could also be broken down into granular tau oligomers as well as filaments derived from recombinant protein (Figure 5a,b of the Supporting Information), further confirming the intermediary role of the granular tau oligomer during PHF formation in the human brain.

In the aged brain, PHF formation may occur when the level of granular tau oligomers increases. Although we found that non-AD brains contained no histologically verified NFTs, these brains did contain granular tau oligomers, albeit fewer than did AD brains. Interestingly, we also detected increased granular tau oligomer levels in brains showing early stage tau pathology. This was consistent with our immunochemical findings showing that granular tau oligomers are immunoreactive for MC1, which was recently reported to be a good indicator of early stage tau pathology in the frontal gyrus, even in the absence of NFTs (*17*). These biochemical data suggested that the formation of a granular tau oligomer precedes NFT formation. Moreover, we found significant differences in the number of granular tau oligomers in Braak stage 0 and I brains (*10*) but not in an oligomer-occupied area per field. We did find, however, significant differences

in oligomer areas in Braak stage 0, III, and V brains, indicating that the oligomers in Braak stage I brains are smaller than those in Braak stage III or V brains. Indeed, in one Braak stage I case that contained a large number of granular tau oligomers, we found smaller-sized granules (data not shown).

Recent results have shown that inhibiting tau expression halfway during the neurodegeneration process in tau transgenic mice induces NFT formation without producing neuronal death (*5*). The findings presented here are not sufficient to resolve this issue. We do know, however, that tau overexpression in tau transgenic mice and in AD brains increases granular tau levels, ultimately leading to NFT formation and neuronal death (*18*−*21*). If the threshold concentration of granular tau that leads to neuronal death is higher than concentrations that lead to NFT formation, inhibiting tau expression could prevent neuronal death, even though NFTs are still generated. If this assumption is true, reducing oligomeric tau might be a promising therapy for various tauopathies, including those associated with aging. Nevertheless, the toxic nature of granular oligomeric tau aggregates needs to be further assessed.

ACKNOWLEDGMENT

We thank Dr. Hara for permitting us to use the NanoscopeIIIa, Drs. Kobayashi and Hayakawa for permitting us to use the Zetasizer, Mr. Usui and Miss Ohtsuki for MS spectroscopy, and Mr. Morishita for amino acid hydrolysis.

SUPPORTING INFORMATION AVAILABLE

Sarcosyl insoluble tau aggregates (Figure 1), temporal changes in in vitro tau aggregation (Figures 2 and 3), details of granular tau oligomer purification from human brain (Figure 4), and tau filament breakdown by continuous AFM imaging (Figure 5). This material is available free of charge via the Internet at http://pubs.acs.org.

REFERENCES

1. Braak, H., and Braak, E. (1997) Frequency of stages of Alzheimer-related lesions in different age categories, *Neurobiol. Aging 18*, 351−357.
2. Lee, V. M., Goedert, M., and Trojanowski, J. Q. (2001) Neurodegenerative tauopathies, *Annu. Rev. Neurosci. 24*, 1121−1159.
3. Ihara, Y. (2001) PHF and PHF-like fibrils: Cause or consequence? *Neurobiol. Aging 22*, 123−126.
4. Reed, L. A., Wszolek, Z. K., and Hutton, M. (2001) Phenotypic correlations in FTDP-17, *Neurobiol. Aging 22*, 89−107.
5. Santacruz, K., Lewis, J., Spires, T., Paulson, J., Kotilinek, L., Ingelsson, M., Guimaraes, A., DeTure, M., Ramsden, M., McGowan, E., Forster, C., Yue, M., Orne, J., Janus, C., Mariash, A., Kuskowski, M., Hyman, B., Hutton, M., and Ashe, K. H. (2005) Tau suppression in a neurodegenerative mouse model improves memory function, *Science 309*, 476−481.
6. Barghorn, S., and Mandelkow, E. (2002) Toward a unified scheme for the aggregation of tau into Alzheimer paired helical filaments, *Biochemistry 41*, 14885−14896.
7. Hasegawa, M., Smith, M. J., and Goedert, M. (1998) Tau proteins with FTDP-17 mutations have a reduced ability to promote microtubule assembly, *FEBS Lett. 437*, 207−210.
8. Friedhoff, P., Schneider, A., Mandelkow, E. M., and Mandelkow, E. (1998) Rapid assembly of Alzheimer-like paired helical filaments from microtubule-associated protein tau monitored by fluorescence in solution, *Biochemistry 37*, 10223−10230.
9. Yoshiike, Y., Tanemura, K., Murayama, O., Akagi, T., Murayama, M., Sato, S., Sun, X., Tanaka, N., and Takashima, A. (2001) New insights on how metals disrupt amyloid β-aggregation and their effects on amyloid-β cytotoxicity, *J. Biol. Chem. 276*, 32293−32299.
10. Maeda, S., Sahara, N., Saito, Y., Murayama, S., Ikai, A., and Takashima, A. (2006) Increased levels of granular tau oligomers: An early sign of brain aging and Alzheimer's disease, *Neurosci. Res. 54*, 197−201.
11. Kayed, R., Head, E., Thompson, J. L., McIntire, T. M., Milton, S. C., Cotman, C. W., and Glabe, C. G. (2003) Common structure of soluble amyloid oligomers implies common mechanism of pathogenesis, *Science 300*, 486−489.
12. George, A., and Wilson, W. W. (1994) Predicting protein crystallization from a dilute solution property, *Acta Crystallogr. D50*, 361−365.
13. Schweers, O., Schonbrunn-Hanebeck, E., Marx, A., and Mandelkow, E. (1994) Structural studies of tau protein and Alzheimer paired helical filaments show no evidence for β-structure, *J. Biol. Chem. 269*, 24290−24297.
14. Greenberg, S. G., and Davies, P. (1990) A preparation of Alzheimer paired helical filaments that displays distinct tau proteins by polyacrylamide gel electrophoresis, *Proc. Natl. Acad. Sci. U.S.A. 87*, 5827−5831.
15. Chirita, C. N., Congdon, E. E., Yin, H., and Kuret, J. (2005) Triggers of full-length tau aggregation: A role for partially folded intermediates, *Biochemistry 44*, 5862−5872.
16. Baskakov, I. V., Legname, G., Baldwin, M. A., Prusiner, S. B., and Cohen, F. E. (2002) Pathway complexity of prion protein assembly into amyloid, *J. Biol. Chem. 277*, 21140−21148.
17. Haroutunian, V., Davies, P., Vianna, C., Buxbaum, J. D., and Purohit, D. P. (2005) Tau protein abnormalities associated with the progression of alzheimer disease type dementia, *Neurobiol. Aging* (in press).
18. Tatebayashi, Y., Miyasaka, T., Chui, D. H., Akagi, T., Mishima, K., Iwasaki, K., Fujiwara, M., Tanemura, K., Murayama, M., Ishiguro, K., Planel, E., Sato, S., Hashikawa, T., and Takashima, A. (2002) Tau filament formation and associative memory deficit in aged mice expressing mutant (R406W) human tau, *Proc. Natl. Acad. Sci. U.S.A. 99*, 13896−13901.
19. Tanemura, K., Akagi, T., Murayama, M., Kikuchi, N., Murayama, O., Hashikawa, T., Yoshiike, Y., Park, J. M., Matsuda, K., Nakao, S., Sun, X., Sato, S., Yamaguchi, H., and Takashima, A. (2001) Formation of filamentous tau aggregations in transgenic mice expressing V337M human tau, *Neurobiol. Dis. 8*, 1036−1045.
20. Tanemura, K., Murayama, M., Akagi, T., Hashikawa, T., Tominaga, T., Ichikawa, M., Yamaguchi, H., and Takashima, A. (2002) Neurodegeneration with tau accumulation in a transgenic mouse expressing V337M human tau, *J. Neurosci. 22*, 133−141.
21. Brandt, R., Hundelt, M., and Shahani, N. (2005) Tau alteration and neuronal degeneration in tauopathies: Mechanisms and models, *Biochim. Biophys. Acta 1739*, 331−354.

BI061359O

J Neuropathol Exp Neurol

Vol. 66, No. 6
June 2007
pp. 469–480

ORIGINAL ARTICLE

Hematopoietic Prostaglandin D Synthase and DP_1 Receptor Are Selectively Upregulated in Microglia and Astrocytes Within Senile Plaques From Human Patients and in a Mouse Model of Alzheimer Disease

Ikuko Mohri, MD, PhD, Keiichi Kadoyama, PhD, Takahisa Kanekiyo, MD, Yo Sato, PhD, Kuriko Kagitani-Shimono, MD, PhD, Yuko Saito, MD, PhD, Kinuko Suzuki, MD, Takashi Kudo, MD, PhD, Masatoshi Takeda, MD, PhD, Yoshihiro Urade, PhD, Shigeo Murayama, MD, PhD, and Masako Taniike, MD, PhD

Abstract

Prostaglandin (PG) D_2 is produced in activated microglia by the action of hematopoietic PGD synthase (HPGDS) and plays important roles in neuroinflammation. Because the fact that neuroinflammation accelerates progression of Alzheimer disease (AD) has been documented, we investigated whether PGD_2 is also involved in the pathology of AD. Here, we report that the level of the mRNA of the receptor for PGD_2 (DP_1) was increased in AD brains compared with the level in non-AD brains. Immunocytochemical analysis showed HPGDS expression to be localized in the microglia surrounding senile plaques. In situ hybridization studies revealed that DP_1 mRNA was specifically localized in microglia and reactive astrocytes within senile plaques of AD brains. In the brain of Tg2576 mice, a model of AD, HPGDS and DP_1 proteins were mainly localized immunocytochemically in microglia and astrocytes in the plaques, and the levels of their mRNAs increased in parallel with amyloid β deposition. These results indicate that PGD_2 may act as a mediator of plaque-associated inflammation in AD brain and may explain the pharmacologic mechanisms underlying the favorable response of patients with AD to nonsteroidal anti-inflammatory drugs.

Key Words: Alzheimer disease, Amyloid β, Gliosis, Neuroinflammation, Nonsteroidal anti-inflammatory drugs (NSAIDs), Prostanoid, Tg2576 mouse.

INTRODUCTION

Alzheimer disease (AD) is the most common form of dementia. The cognitive decline in patients with AD is associated with neuronal degeneration, the appearance of neurofibrillary tangles, and the formation of senile plaques (1). It has been reported that inflammatory responses, including the production of proinflammatory cytokines and prostaglandins by activated microglia and astroglia, play important roles in the pathology of AD (2–5). Senile plaques arise from the excessive accumulation, aggregation, and deposition of amyloid β (Aβ) peptide, which triggers the activation of microglia and astrocytes around the senile plaques. Tg2576 mice overexpressing human APP695 with the "Swedish" mutation (a murine model of AD) develop memory deficits and senile plaques as they age (6). These animals show a rapid increase in Aβ deposition starting around 6 months and amyloid plaques beginning at 9 to 12 months (7).

We recently reported that activated microglia express hematopoietic prostaglandin (PG) D synthase (HPGDS) and that PGD_2 produced by HPGDS promotes neuroinflammation in a mouse model of Krabbe disease (8). These discoveries

From Department of Mental Health and Environmental Effects Research (IM, M. Taniike), The Research Center for Child Mental Development, Osaka University Graduate School of Medicine, Suita, Osaka, Japan; Department of Developmental Medicine (Pediatrics) (IM, TK, KK-S, M. Taniike), Osaka University Graduate School of Medicine, Suita, Osaka, Japan; Department of Molecular Behavioral Biology (IM, KK, Y. Sato, YU), Osaka Bioscience Institute, Suita, Osaka, Japan; Department of Pathology and Laboratory Medicine (IM, KS), School of Medicine, University of North Carolina at Chapel Hill, Chapel Hill, North Carolina; Departments of Neuropathology and Pathology (Y. Saito, SM), Tokyo Metropolitan Geriatric Hospital, Itabashi-ku, Tokyo, Japan; and Division of Psychiatry and Behavioral Proteomics (TK, M. Takeda), Department of Post-Genomics and Diseases, Course of Advanced Medicine, Osaka University, Graduate School of Medicine, Suita, Osaka, Japan.

Drs. Mohri, Kadoyama, and Kanekiyo contributed equally to this work.

Drs. Urade, Murayama, and Taniike contributed equally in supervising this project.

Send correspondence and reprint requests to: Masako Taniike, MD, PhD, Department of Mental Health and Environmental Effects Research, The Research Center for Child Mental Development, Osaka University Graduate School of Medicine, 2-2, D-5, Yamadaoka, Suita, Osaka 565-0871, Japan; E-mail: masako@ped.med.osaka-u.ac.jp

This study was supported in part by research grants from the Ministry of Education, Culture, Sports, Science, and Technology of Japan (M. Taniike); the Osaka Medical Research Foundation for Incurable Diseases (M. Taniike), Japan Science and Technology Corporation (YU); Takeda Science Foundation (YU); Aid for Scientific Research on Priority Areas Advanced Brain Science Project from the Ministry of Education, Culture, Sports, Science, and Technology of Japan (SM, Y. Saito); Aid for Longevity Sciences from the Ministry of Health, Labor, and Welfare (SM); and Aid for Long-Term Comprehensive Research on Age-Associated Dementia from Tokyo Metropolitan Institute of Gerontology (SM), and Osaka City.

prompted us to clarify whether PGD_2 is also involved in the plaque-associated inflammation in the AD brain. A determination of the mRNA contents of all known brain prostanoid synthases and receptors showed that HPGDS and DP1 mRNAs were selectively expressed to a higher level in AD brains compared with their levels in age-matched control patients. This overexpression was localized to reactive astrocytes and microglia closely associated with senile plaques, suggesting that HPGDS/PGD_2/DP_1 signaling may accelerate chronic local inflammation around plaques in AD. We also found that HPGDS and DP_1 mRNAs were selectively expressed in reactive astrocytes and microglia closely associated with senile plaques in the AD brains and brains of Tg2576 mouse. Our findings suggest that HPGDS/PGD_2/DP_1 signaling may accelerate chronic local inflammation around senile plaques in the AD brain.

MATERIALS AND METHODS

Human Tissue Source

Human brain tissues were obtained from Tokyo Metropolitan Brain Bank for Aging Research according to the neuropathologic protocols described elsewhere (9). We obtained tissue fresh at autopsy and stored it at −80°C, and, to avoid RNA degradation, we selected samples with as short a postmortem interval before autopsy as possible. The storage period was 2 to 32 months and 2 to 31 months for AD and control brains, respectively, and the storage period was not significantly different between the 2 groups.

Fifteen brains each from AD patients and control patients without clinicopathologic evidence of AD were the basis of the present work. The diagnosis of AD was based on the following criteria: 1) clinical dementia rating of ≥1 (10); 2) the topographical distribution of senile plaques matching Braak stage C; and 3) of neurofibrillary tangles equal to or above stage IV, as reported elsewhere (9). The selection criterion for control patients was a clinical dementia rating score of 0, senile plaque stage 0 or A, and a neurofibrillary tangle stage lower than stage II. The profiles of AD and control patients are listed in Table 1. Subjects with AD were 70 to 93 years old (82.6 years on average), and the postmortem delay ranged from 1.5 to 17 hours (average of 8.5 hours). The age of non-AD control patients was 71 to 91 years (79.5 on average), and the postmortem delay was 2.3 to 14.8 hours (average of 12.1 hours).

The tissues were either snap-frozen in liquid nitrogen or powdered dry ice or immediately fixed in 4% paraformaldehyde (Sigma, St. Louis, MO) for 2 days and processed into paraffin blocks. Paraffin or frozen sections of 6-μm thickness from the frontal cortex and the hippocampus were cut with a cryostat (CM1850; Leica Microsystems, Wetzlar, Germany) and microtome (RM 2035; Leica), and used for immunohistochemical studies. Snap-frozen tissues, that were en face to the paraffin sections, were also used for quantitative reverse transcriptase (RT)-polymerase chain reaction (PCR) analysis of mRNA expression. The frontal cortex was selected for this purpose, because the difference in the number of senile plaques was most prominent there between AD and control groups. This study was approved by the institutional review boards of Osaka University Graduate School of Medicine, Tokyo Metropolitan Geriatric Hospital, Tokyo Metropolitan Institute of Gerontology, and Osaka Bioscience Institute.

Mice

All animal experiments were performed in accordance with Japanese law for the protection of experimental animals and conformed to the regulations issued by the National Institutes of Health and the Society for Neuroscience. Homozygous Tg2576 mice were purchased from Taconic (Hudson, NY) and maintained by interbreeding.

Quantitative Reverse Transcriptase-Polymerase Chain Reaction Analysis of mRNA

By quantitative RT-PCR analysis, we determined the mRNA contents of enzymes involved in prostanoid synthesis, including cyclooxygenase (COX)-1, COX-2, HPGDS, lipocalin-type PGD synthase (L-PGDS), microsomal PGE synthases (mPGES-1 and mPGES-2), cytosolic PGE synthase (cPGES), PGF synthase, prostacyclin synthase, thromboxane (TX) A synthase, and those of prostanoid receptors for PGD_2 (DP_1 and DP_2), PGE_2 (EP_1, EP_2, EP_3, and EP_4), $PGF_{2\alpha}$ (FP), PGI_2 (IP), and TXA_2 (TP), as well as the mRNA content of cytosolic phospholipase A_2 ($cPLA_2$) and peroxisome proliferator-activated receptor (PPAR)-γ. After removal of the pia-arachnoid membrane, total RNA was prepared from the frontal cortex of 17 AD patients and 12 control patients by using ISOGEN (Nippon Gene, Tokyo, Japan) according to the manufacturer's instructions. In the mouse model, 3 each of Tg2576 and age-matched wild-type mice at ages 6 months, 1 year, and 2 years were subjected to quantitative RT-PCR for determination of COX-1, COX-2, HPGDS, DP_1, and DP_2 mRNA levels. All primers were synthesized by Sigma-Aldrich Japan (Tokyo, Japan). First-strand cDNAs were synthesized from 1 μg of total RNA by using avian myeloblastosis virus reverse transcriptase (Takara, Kyoto, Japan) and oligo dT-adaptor primer (Takara) at 50°C for 40 minutes after denaturation at 72°C for 3 minutes. The cDNA was amplified by use of a real-time PCR LightCycler system (Roche Diagnostics, Indianapolis, IN), a LightCycler-FastStart DNA Master SYBR Green I (Roche Diagnostics), and gene-specific primers under the following conditions: an initial denaturation at 94°C for 10 minutes, followed by 40 cycles of denaturation at 94°C for 15 seconds, annealing for 5 seconds, and extension at 72°C for 10 seconds. The oligonucleotide primers and annealing temperatures used are shown in Table 2. All oligonucleotide primers were synthesized by Sigma Genosys Japan (Tokyo, Japan). PCR products were evaluated by melting-curve analysis following the manufacturer's instructions, checked after agarose gel electrophoresis, and sequenced. All values were corrected with reference to the value for glyceraldehyde-3-phosphate dehydrogenase (G3PDH), used as an internal standard.

Immunocytochemistry

Rabbit polyclonal antibodies against human HPGDS, L-PGDS, and mPGES-1 (11), and rabbit polyclonal

TABLE 1. Clinicopathologic Features of the Patients

Patient	Age	Sex	Neuropathologic Diagnosis	SP	NFT	CERAD	Postmortem Interval (hours)	Cause of Death
C1	91	F	Unremarkable	A	II	Normal	13:25	DIC, Heart failure
C2	83	M	Unremarkable	0	I	Normal	17:43	AMI
C3	82	M	Unremarkable	A	I	Normal	12:16	COPD
C4	81	M	Unremarkable	0	I	Normal	2:14	MDS, congestive heart failure
C5	80	M	Unremarkable	0	II	Normal	8:50	Hepatocellular carcinoma
C6	79	F	Unremarkable	A	I	Normal	2:52	AAA, COPD
C7	78	M	Unremarkable	0	II	Normal	2:30	COPD, sudden death
C8	78	M	Unremarkable	0	I	Normal	9:35	Sepsis
C9	78	F	Unremarkable	A	I	Normal	2:39	Sepsis
C10	77	M	Unremarkable	0	I	Normal	10:25	Lung cancer (small cell carcinoma)
C11	76	M	Unremarkable	A	II	Normal	5:14	Lung cancer (small cell carcinoma)
C12	71	M	Unremarkable	0	I	Normal	13:54	Severe pneumonia, sepsis
AD1	93	M	AD	C	V	Definite	1:47	Leiomyosarcoma of stomach, abdominal dissemination
AD2	91	M	AD	C	IV	Definite	9:40	Carcinoma of the bile duct
AD3	88	F	AD	C	VI	Definite	5:25	AMI, sepsis
AD4	87	M	AD	C	VI	Definite	3:17	Lung cancer
AD5	87	F	AD	C	V	Definite	16:56	MRSA sepsis
AD6	85	F	AD	C	VI	Definite	16:40	Ileus, pneumonia
AD7	84	M	AD	C	V	Definite	9:50	Pneumonia, ileus
AD8	84	F	AD	C	V	Definite	8:41	Cholecystitis
AD9	84	F	AD	C	IV	Definite	9:35	Congestive heart failure, OMI
AD10	82	F	AD	C	VI	Definite	4:14	Perforation of gastric ulcer
AD11	82	F	AD	C	V	Definite	8:53	Sudden death
AD12	81	M	AD	C	IV	Definite	12:57	AMI, septal perforation
AD13	81	M	AD	C	VI	Definite	6:00	Pulmonary emphysema, respiratory failure
AD14	76	M	AD	C	VI	Definite	15:47	Sepsis, early gastric cancer
AD15	75	M	AD	C	VI	Definite	9:54	Pneumonia
AD16	74	M	AD	C	VI	Definite	5:12	Pneumonia, DIC
AD17	70	M	AD	C	V	Definite	11:42	Hodgkin lymphoma, pneumonia

The diagnosis of AD was based on a clinical dementia rating (CDR) of ≥1, topographical distribution of senile plaques (SP) matching Braak stage C, and that of neurofibrillary tangles (NFTs) equal to or above stage IV (9). The selection criterion for control patients was a CDR score of 0, senile plaque stage 0 or A, and an NFT stage lower than stage II.

AAA, abdominal aortic aneurysm; AD, Alzheimer disease; AMI, acute myocardial infarction; CERAD, Consortium to Establish A Registry for Alzheimer's Disease; COPD, chronic obstructive pulmonary disease; DIC, disseminated intravascular coagulation; MDS, myelodysplastic syndrome; MRSA, methicillin-resistant *Staphylococcus aureus*; OMI, occlusive mesenteric ischemia.

(0.1 μg/mL) and rat monoclonal (0.2 μg/mL) anti-mouse HPGDS antibodies (12) were raised and purified in Osaka Bioscience Institute. The specificity of each antiserum (1:1000 dilution) was confirmed by the disappearance of immunoreactivity after incubation of the antiserum with an excess amount of the corresponding purified recombinant immunogen. The other primary antibodies used in this study were as follows: anti-cow glial fibrillary acidic protein (GFAP) (1:5000 dilution; DakoCytomation, Glostrup, Denmark) for astrocytes; anti-human CD68 antibody (1:100 dilution; DakoCytomation) and anti-Iba1 (a generous gift of Dr. Shinichi Kousaka, National Center of Neurology and Psychiatry, Japan) for microglia/macrophages; and anti-human Aβ (11-28) antibody (1:100 dilution; IBL, Gunma, Japan) for detecting amyloid plaques.

Tg2576 and control mice were used for immunocytochemical analysis. Under deep ether anesthesia, the mice were perfused via the heart with physiologic saline, followed by 4% paraformaldehyde in 0.1 M sodium phosphate (pH 7.4) for 10 minutes. The brains were removed and postfixed in the same fixative overnight. Coronal slices were taken and routinely embedded in paraffin. Additionally, 2 each of Tg2576 and control mice were perfused with physiologic saline only and processed for the preparation of fresh-frozen sections. Both paraffin and frozen sections (5-μm thickness) were mounted on 3-aminopropyltriethoxysilane-coated slides.

Deparaffinized sections were preincubated with 0.3% H_2O_2 (Wako, Osaka, Japan) in methanol followed by PBS containing 0.2% Triton X-100 (Nakarai Tesque, Kyoto, Japan). After pretreatment with 0.1% trypsin (Sigma) at 37°C for 15 minutes, they were sequentially incubated with primary antibody, biotinylated secondary antibody (2 μg/mL; Vector Laboratories, Burlingame, CA), and avidin-biotin-complex (ABC) by using an ABC elite system (Vector Laboratories) according to the manufacturer's protocol.

For double immunostaining, deparaffinized sections were incubated at 4°C overnight with either anti-GFAP or anti-CD68 antibody together with rabbit anti-human HPGDS

TABLE 2. Primer Sequences and Annealing Temperatures Used for Quantitative Reverse Transcriptase-Polymerase Chain Reaction Analysis

	Primer	Primer Sequence	Annealing Temperature (°C)
Human			
HPGDS	Forward	5′-GAATAGAACAAGCTGACTGGC-3′	57
	Reverse	5′-AGCCAAATCTGTGTTTTTGG-3′	
L-PGDS	Forward	5′-CAGGAAAAACCAGTGTGAGACC-3′	57
	Reverse	5′-AGAGGGTGGCCATGCGGAAG-3′	
mPGES-1	Forward	5′-CTGCTGGTCATCAAGATGTACG-3′	59
	Reverse	5′-ACACACCGTGGCCTACCTGGG-3′	
mPGES-2	Forward	5′-TACCAGTACAAGACGTGTCCCTTC-3′	56
	Reverse	5′-GGTAGTAGGTGATGATCTCTTCCAG-3′	
cPGES	Forward	5′-TACATTCAGTTGTCTCGGAGGAAG-3′	56
	Reverse	5′-ATCATCTGCTCCATCTACTTCTGG-3′	
PGFS	Forward	5′-GGCAGTGTGAAGAGAGAAGACATA-3′	56
	Reverse	5′-AATCCTGCATCCTTACACTTCTCC-3′	
DP_1	Forward	5′-CCTCTGAAGAAGCAGAAGACCT-3′	56
	Reverse	5′-CCTCAGCTTACCACAGAGTGA-3′	
DP_2	Forward	5′-CTCCTCCATCTTCTTTCTCAACA-3′	56
	Reverse	5′-TTCAGGAGCAGCACATTGTAGTA-3′	
EP_1	Forward	5′-AACCTGAGCCTGGCGGGCGAGGCGA-3′	55
	Reverse	5′-AGAAGACCATGCAGCCGCCCAGGAA-3′	
EP_2	Forward	5′-GTGCGAGTATTCGTCAACCAGT-3′	57
	Reverse	5′-TGACATGGCAGAAGATGTCCTT-3′	
EP_3	Forward	5′-GACAGTCACCTTTTCCTGCAAC-3′	57
	Reverse	5′-CCAGGCGAACAGCTATTAAGAA-3′	
EP_4	Forward	5′-CCTGAGAAAGACAGTGCTCAGTAA-3′	55
	Reverse	5′-CTGAGGTCTCTGATATTCGCAAAG-3′	
FP	Forward	5′-ATTTAGACAGAAGTCCAAGGCATC-3′	56
	Reverse	5′-AACAAGCACACACCACTTAACATC-3′	
G3PDH	Forward	5′-TGAACGGGAAGCTCACTGG-3′	60
	Reverse	5′-TCCACCACCCTGTTGCTGTA-3′	
Mouse			
COX-1	Forward	5′-AGATAATCTGGAACGACAGTATCACC-3′	60
	Reverse	5′-CATAGTCCACCAGCATAGAAGTGTTA-3′	
COX-2	Forward	5′-AACTGTACCCTGCCCTGCTGGTGGAAAA-3′	59
	Reverse	5′-AGATGACATTAACCCTACAGTACTAATC-3′	
HPGDS	Forward	5′-GAATAGAACAAGCTGACTGGC-3′	57
	Reverse	5′-AGCCAAATCTGTGTTTTTGG-3′	
DP_1	Forward	5′-TTTGGGAAGTTCGTGCAGTACT-3′	56
	Reverse	5′-GCCATGAGGCTGGAGTAGA-3′	
DP_2	Forward	5′-TGGCCTTCTTCAACAGCGT-3′	56
	Reverse	5′-ACGCAGTTGGGGAATTCG-3′	
G3PDH	Forward	5′-TGAACGGGAAGCTCACTGG-3′	60
	Reverse	5′-TCCACCACCCTGTTGCTGTA-3′	

COX, cyclooxygenase; cPGES, cytosolic PGES; DP_1 and DP_2, prostanoid receptors for PGD_2; EP_1, EP_2, EP_3, and EP_4, prostanoid receptors for PGE_2; FP, prostanoid receptor for $PGF_{2\alpha}$; G3PDH, glyceraldehyde-3-phosphate dehydrogenase; HPGDS, hematopoietic prostaglandin (PG) D synthase; L-PGDS, lipocalin-type PGD synthase; mPGES, microsomal PGE synthase; PGFS, PGF synthase.

antiserum. The sections were then reacted with alkaline phosphatase-conjugated anti-mouse IgG antibody (2 μg/mL; Aurora, Cambridge, UK) and biotin-conjugated anti-rabbit IgG antibody (Vector Laboratories), followed by ABC. The reaction products of horseradish peroxidase and alkaline phosphatase activities were visualized with diaminobenzidine (Dotite, Kumamoto, Japan) and naphthol AS-BI phosphate (Sigma) coupled to hexazotized new fuchsin (Merck, Darmstadt, Germany), respectively, as substrates.

All sections were analyzed, and images were obtained with an Olympus BX51 microscope (Olympus, Tokyo, Japan) equipped with a DP50 digital camera. The digital images were adjusted to an appropriate figure size required but were otherwise not processed.

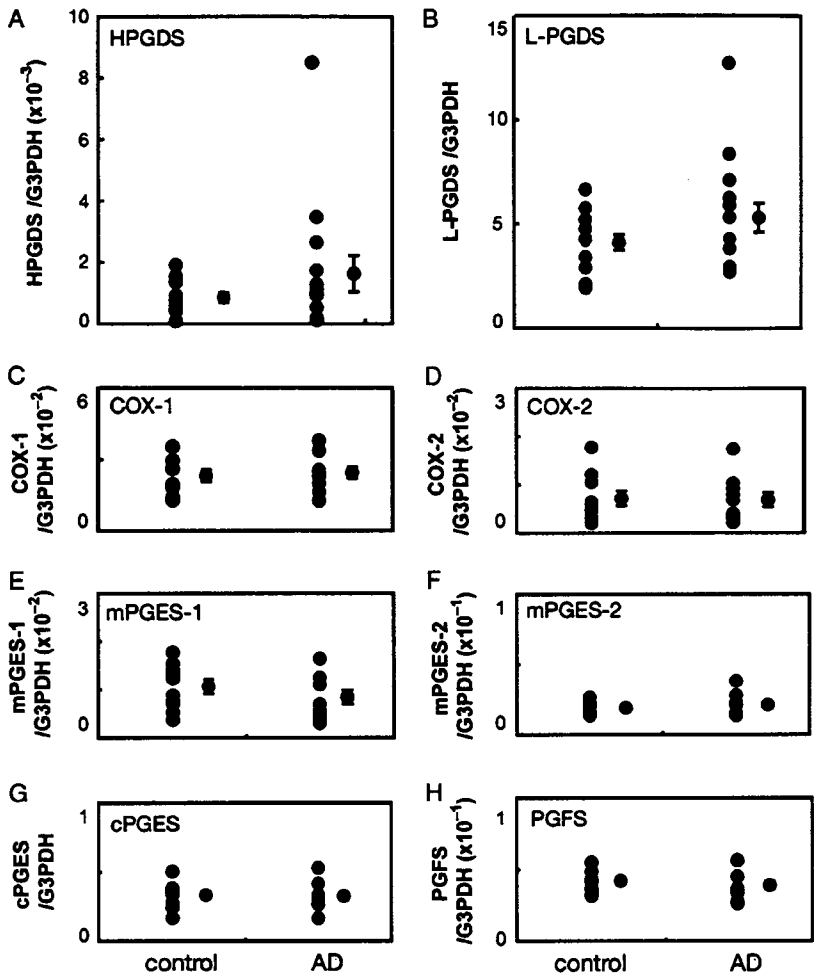

FIGURE 1. (A–H) Expression of prostaglandin synthase mRNA in the frontal cortex of AD (n = 17) and control brains (n = 12), as evaluated by quantitative RT-PCR analysis. The numbers of copies relative to those of G3PDH are shown. The mean values and SE are indicated by the crossbars. AD, Alzheimer disease; COX, cyclooxygenase; cPGES, cytosolic PGES; HPGDS, hematopoietic prostaglandin (PG) D synthase; G3PDH, glyceraldehyde-3-phosphate dehydrogenase; L-PGDS, lipocalin-type PGD synthase; mPGES, microsomal PGE synthase; PGFS, PGF synthase.

In Situ Hybridization

In situ hybridization was performed by using a digoxigenin (DIG)-anti-DIG technique. For preparation of the human DP_1 riboprobe, a 484-base pair fragment was amplified by use of FastStart Taq DNA polymerase (Roche Diagnostics) with human DP_1-specific primers (forward, 5′-GGGGTACTCTGTGCTCTACTCCAG-3′ and reverse, 5′-ACTGGATTCCATGTTAGTGGAATTG-3′), subcloned into pGEM-T Easy vector (Promega, Madison, WI), and converted into the corresponding RNA. Five-micrometer-thick cryosections were fixed in 10% formalin (Wako) for 1 hour and hybridized at 58°C for 16 hours with the DIG-labeled riboprobe for DP_1 in 50% formamide (Wako), 5 × saline sodium citrate, 5 × Denhardt's solution, 0.25 mg/mL yeast tRNA, and 0.5 mg/mL herring sperm DNA. After the sections had been washed with PBS, the DIG-labeled RNA was detected by using a Genius DNA labeling and detection kit (Roche Diagnostics) according to the manufacturer's protocol.

For identification of DP_1-expressing cells, the sections were reacted with the DP_1-specific riboprobe and then immunostained with either anti-human GFAP antibody, anti-human CD68 antibody, or anti-human Aβ (11-28) antibody detected by using either immunofluorescence or immunoperoxidase. For fluorescence labeling, a biotinylated riboprobe was used in place of the DIG-labeled riboprobe. For double immunofluorescence, we confirmed the colocalization by omitting 1 of the first antibodies during the process.

Primary Cultures of Mouse Microglia and Astrocytes

We prepared primary cultures of microglia from wild-type mouse brains at postnatal day 1. Cerebral cortices were dissected, and the leptomeninges were completely removed.

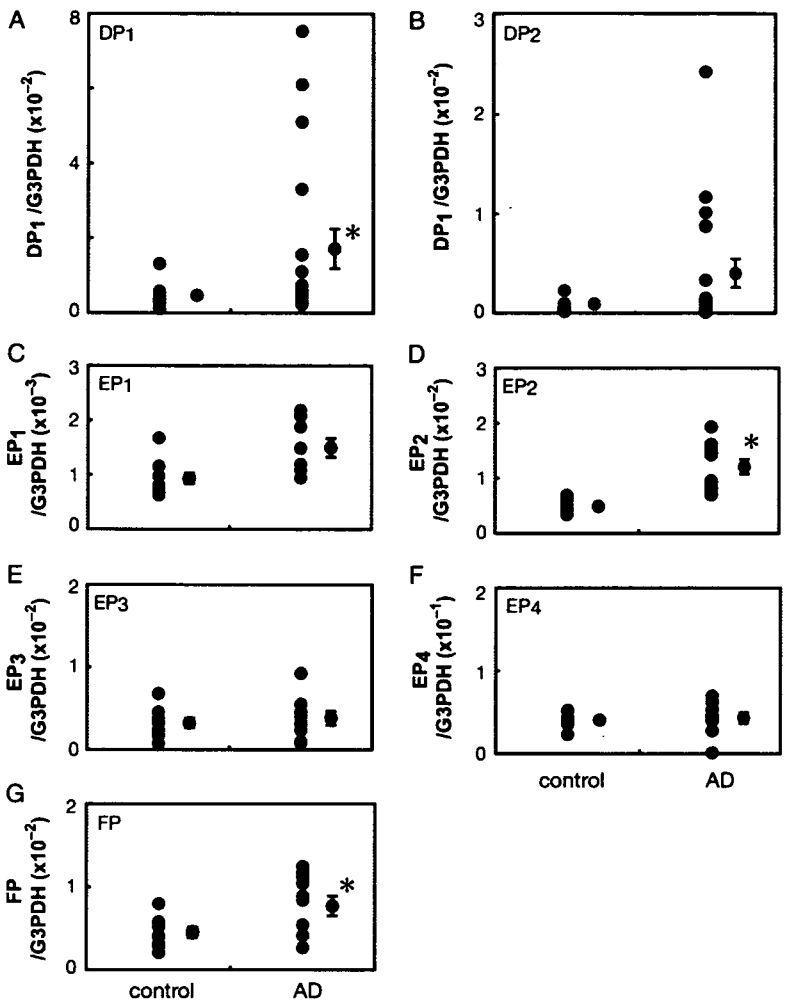

FIGURE 2. (A–G) mRNA expression of prostanoid receptors in the frontal cortex of Alzheimer disease (AD) (n = 17) and control brains (n = 12), as determined by quantitative RT-PCR analysis. The numbers of copies relative to glyceraldehyde-3-phosphate dehydrogenase (G3PDH) are shown. The mean values and SE are indicated by the crossbars. *, $p < 0.05$.

The tissues were minced, suspended in PBS (GIBCO, Grand Island, NY) containing 0.05% trypsin (GIBCO) and 0.01% DNase I (Sigma), and then incubated for 10 minutes at 37°C. After incubation and centrifugation, the cell pellets were washed 3 times with PBS. The cells were then filtered through a 75-μm nylon mesh, centrifuged, suspended in Dulbecco's modified Eagle's medium (Nakalai Tesque) containing 10% fetal bovine serum (JRH Biosciences, Lenexa, KS), 100 IU/mL penicillin (GIBCO), and 100 μg/mL streptomycin (GIBCO), and transferred to culture dishes. For microglial cultures, the medium was changed to Dulbecco's modified Eagle's medium containing 10% fetal bovine serum after a 24-hour culture period. This medium was exchanged for fresh medium twice weekly thereafter. The supernatants including microglial cells were collected and subcultured at 1×10^5 cells/well (6-well plate). After incubation in Dulbecco's modified Eagle's medium without fetal bovine serum for 6 hours, the microglia were stimulated by the addition of Aβ (1-40) (Peptide Institute, Osaka, Japan) for 24 hours. After the cells had been washed with PBS, RNA was extracted from them and subjected to quantitative RT-PCR.

Data Analysis

The difference of means among groups of data was analyzed by analysis of variance. Statistical significance was established at the level of $p < 0.05$ or 0.01.

RESULTS

Expression of Prostanoid-Producing Enzymes in Alzheimer Disease Brains

Using the frontal cortex obtained from AD and control patients, we examined the mRNA expression level of all enzymes involved in prostanoid synthesis. Quantitative

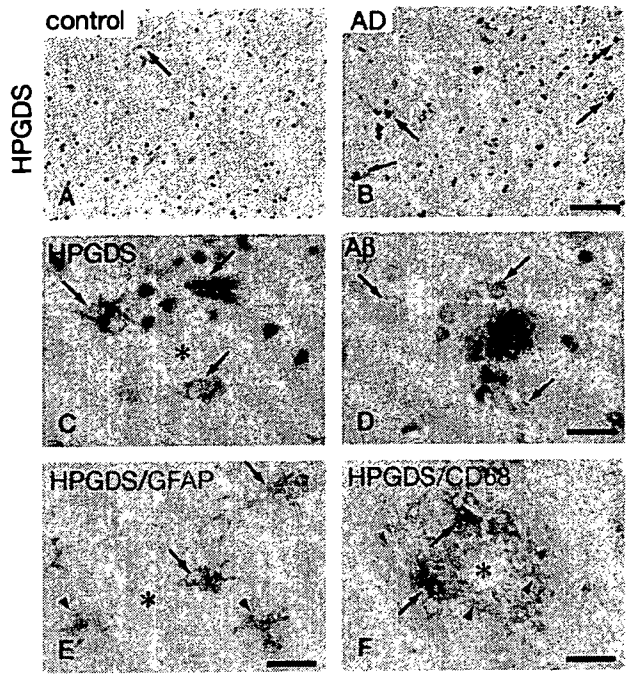

FIGURE 3. Expression of hematopoietic prostaglandin synthase (HPGDS) in Alzheimer disease (AD) and control brains. In the following panels, asterisks indicate the presence of senile plaques. **(A, B)** Immunohistochemical analysis of HPGDS in control **(A)** and AD **(B)** brains. Arrows point to HPGDS-positive cells. Scale bar = 50 μm. **(C, D)** Immunostaining for HPGDS **(C)** and amyloid β (Aβ) **(D)** associated with the senile plaques in an AD brain. The same cells in the serial sections are indicated by arrows. Scale bar = 20 μm. **(E, F)** Double immunostaining for HPGDS (purple) and glial fibrillary acidic protein (GFAP) (pink, **E**) or CD68 (pink, **F**) in an AD brain. HPGDS-positive/GFAP- **(E)** or CD68-positive **(F)** and HPGDS-negative/GFAP- **(E)** or CD68-positive **(F)** cells are indicated by arrows and arrowheads, respectively. Scale bar = 20 μm.

RT-PCR analysis revealed the mRNA levels of HPGDS (Fig. 1A) and L-PGDS (Fig. 1B) to be elevated in AD brains compared with those of the control brains. However, the mRNA levels of other prostanoid-producing enzymes including COX-1 and -2 (Fig. 1C, D), PGESs including mPGES-1, mPGES-2, and cPGES (Fig. 1E–G), PGF synthase (Fig. 1H), and TXA synthase (data not shown), as well as the mRNA level of $cPLA_2$ (data not shown), were similar between control and AD brains. Prostacyclin synthase mRNA was not detected in either AD or control samples (data not shown).

Increased DP_1 Expression in Alzheimer Disease Brains

Next, we examined the mRNA expression level of all prostanoid receptors thus far identified (Fig. 2) and found that the expression of DP_1 was significantly upregulated in AD brains as compared with that in control brains (Fig. 2A). In 6 of the 17 AD patients, the mRNA level was higher than 2 SD from the mean of control brains, and these values were 2.5- to 16-fold greater than this mean. The mRNA level of DP_2, which is another PGD_2 receptor, was also increased, but not significantly, in AD brains (Fig. 2B). In contrast, the mRNA levels of other prostanoid receptors were almost the same between the 2 groups (Fig. 2C–G) except for the approximately 2-fold increases in EP_2 (Fig. 2D) and FP (Fig. 2G) in AD brains. In addition, the mRNA level of PPARγ, which is a nuclear receptor for PGD_2 metabolites (13), was not significantly different between AD and control brains (data not shown).

Expression of Hematopoietic Prostaglandin D Synthase and DP_1 Is Associated with Senile Plaques in Alzheimer Disease Brains

Because the mRNA levels of HPGDS and DP_1 mRNA were increased in AD brains, as judged from the results of RT-PCR analysis, we investigated the cellular localization of these messages.

Immunocytochemical analysis revealed that anti-HPGDS-immunoreactive cells were greater in number in the AD brain than in the control brain (Fig. 3A, B). Serial immunostaining for HPGDS and Aβ revealed that HPGDS-positive cells were closely associated with Aβ-positive senile plaques (Fig. 3C, D) in the frontal cortex and the hippocampus. HPGDS-positive cells were frequently recognized in relatively small-sized plaques accompanied by activated microglia (Fig. 3B, C) but not in the large "burned out class" of plaques (data not shown). Double immunocytochemical staining revealed that HPGDS was localized in GFAP-positive reactive astrocytes (Fig. 3E) and in CD68-positive microglia (Fig. 3F) associated with the senile plaques, suggesting that HPGDS expression was upregulated

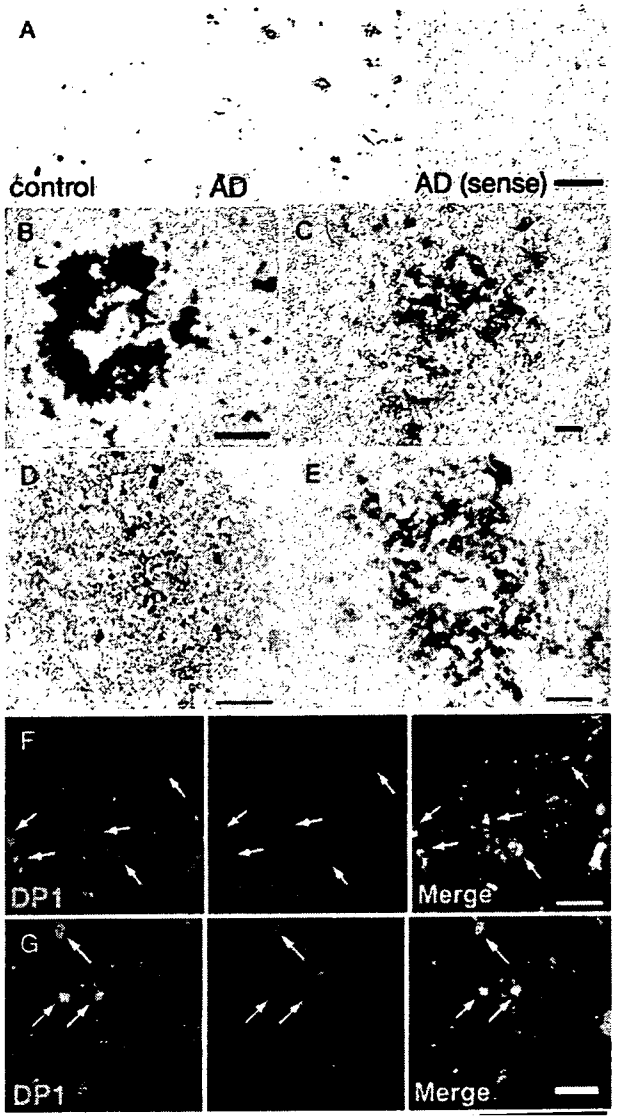

FIGURE 4. (A) In situ hybridization for DP_1 in control and Alzheimer disease (AD) brains. Control (left) and AD brain (middle) sections were incubated with antisense riboprobe. Another AD brain section was incubated with sense riboprobe (right). Scale bar = 100 μm. **(B, C)** In situ hybridization for DP_1 (purple) and immunocytochemistry for amyloid β (Aβ) (pink) in an AD brain. The DP_1-positive cells are uniformly intermingled with Aβ immunoreactivity in the senile plaque **(B)**, and a large-sized DP_1-negative senile plaque is shown **(C)**. Scale bar = 20 μm. **(D, E)** Double staining by in situ hybridization for DP_1 (purple) and immunocytochemistry for glial fibrillary acidic protein (GFAP) (brown, **D**) or CD68 (brown, **E**). Scale bar = 50 μm. **(F, G)** Double fluorescence labeling for DP_1 (green) and GFAP (red, **F**) or CD68 (red, **G**). Double-positive cells are indicated by arrows. Scale bar = 30 μm.

in reactive astrocytes and microglia within the senile plaques. Immunocytochemical analysis revealed that L-PGDS-expressing cells having the same morphologic characteristics as oligodendrocytes, as reported previously (14), were increased in number and were more intensely stained in AD than in control brains; however, the distribution of L-PGDS-positive oligodendrocytes was almost ubiquitous and seemingly unrelated to that of senile plaques (data not shown). mPGES was localized in some neurons of both AD and control brains, but there was no significant difference in intensity of staining or in the number of immunoreactive neurons between the 2 (data not shown).

Upregulation of DP_1 mRNA in AD brains was confirmed by in situ hybridization with a DP_1-specific antisense riboprobe, because antibody specific for human DP_1 is still unavailable. DP_1 mRNA was hardly detected in the control brain (Fig. 4A); however, high signal density was detected in AD brains (Fig. 4A). When we hybridized the sections with the DIG-labeled antisense riboprobe in the presence of a 500-fold excess of nonlabeled antisense riboprobe or with sense riboprobe, no signal was observed in either control or AD brain sections (Fig. 4A, sense). Double labeling for Aβ and DP_1 hybridization revealed that the distribution of the DP_1 signal was closely associated with Aβ immunoreactivity (Fig. 4B). However, the intensity of the DP_1 signal differed among the senile plaques; and the signal was less preferentially observed in large-sized senile plaques (Fig. 4C). Furthermore, double staining with antibodies against glial markers revealed that the DP_1 signal was localized in GFAP-positive reactive astrocytes (Fig. 4D, F) and CD68-positive microglia (Fig. 4E, G) within senile plaques, similar to the distribution of HPGDS shown in Figure 3E and F. These results indicate that expression of HPGDS and DP_1 was increased in reactive astrocytes and microglia within the senile plaques in AD brain and suggest that PGD_2 produced by HPGDS exerts its function through binding to DP_1 in a paracrine or autocrine manner. The preferential expression of these PGD_2-related molecules in the small-sized senile plaques suggests the contribution of PGD_2 to neuroinflammation in the early phase of plaque evolution.

Upregulation of Hematopoietic Prostaglandin D Synthase and DP_1 Expression in Tg2576 Mouse Brain

Next we examined the Tg2576 mouse brain to clarify the relevancy of our findings on human AD brains. In 2-year-old mice, there were numerous amyloid plaques in the cortex of Tg2576 brains (Fig. 5A) but not in that of the wild-type mouse brain (Fig. 5B). The results of the combination of Congo red staining and immunocytochemistry for Iba1, a marker for activated microglia, are shown in Figure 5C and D. Surrounding the amyloid plaques were many Iba1-positive activated microglia (Fig. 5D, arrowheads), which were not seen in the wild-type control. Double labeling with Congo red and anti-GFAP showed that fibers from activated astrocytes surrounded and enclosed amyloid plaques (Fig. 5E, F). These findings indicate that inflammatory responses such as microglial activation and astrogliosis were remarkable around early amyloid plaques in the Tg2576 mouse brain.

Next we investigated the localization of HPGDS and DP_1 in the Tg2576 mouse brain. As in the case of the human

AD brains, HPGDS-positive microglia were common in relatively small plaques (Fig. 5G) but not in the large burned out class of plaques (Fig. 5H). HPGDS and Iba1 double immunofluorescence revealed that HPGDS was expressed in a certain number of Iba1-positive activated microglia (Fig. 5I). DP_1 and GFAP double immunofluorescence revealed that DP_1 was expressed on the astrocytic processes close to the amyloid plaques (Fig. 5J).

Quantitative RT-PCR was performed to evaluate the level of PGD_2-related molecules in Tg2576 mouse brains and age-matched controls at the age of 6 months, 1 year, and 2 years. The expression of COX-1 mRNA was not different between Tg2576 and control mice (Fig. 6A), but that for COX-2 was higher in the Tg2578 mouse starting from the age of 6 months (Fig. 6B). The level of HPGDS mRNA was the same between Tg2576 and wild-type controls until they reached 2 years of age, at which time its level was 1.5 times higher in the Tg2576 mice than in the controls (Fig. 6C). The level of DP_1 mRNA progressively increased in the Tg2576 mouse brain and reached a level 5-times higher than that in the control mice at the age of 2 years (Fig. 6D). In the case of DP_2, its mRNA level progressively increased starting before the age of 1 year compared with that of the age-matched controls (Fig. 6E). These lines of evidence show that HPGDS and DP_1 expression was associated with the small senile plaques and that the increase in DP_2 receptors was more marked than that of HPGDS in the mouse model as in human AD.

To examine whether Aβ could directly stimulate the production of HPGDS in microglia, we performed an in vitro study using primary cultures of microglia obtained from normal neonatal mouse brains. We measured the level of HPGDS mRNA in these cultures before and after stimulating the cells with Aβ(1-42) at concentrations from 0 to 1000 nM. As shown in Figure 6F, the level of HPGDS mRNA did not increase when a 1 nM concentration of Aβ(1-42) was tested but did significantly increase when a 10 nM concentration or higher was used. However, no

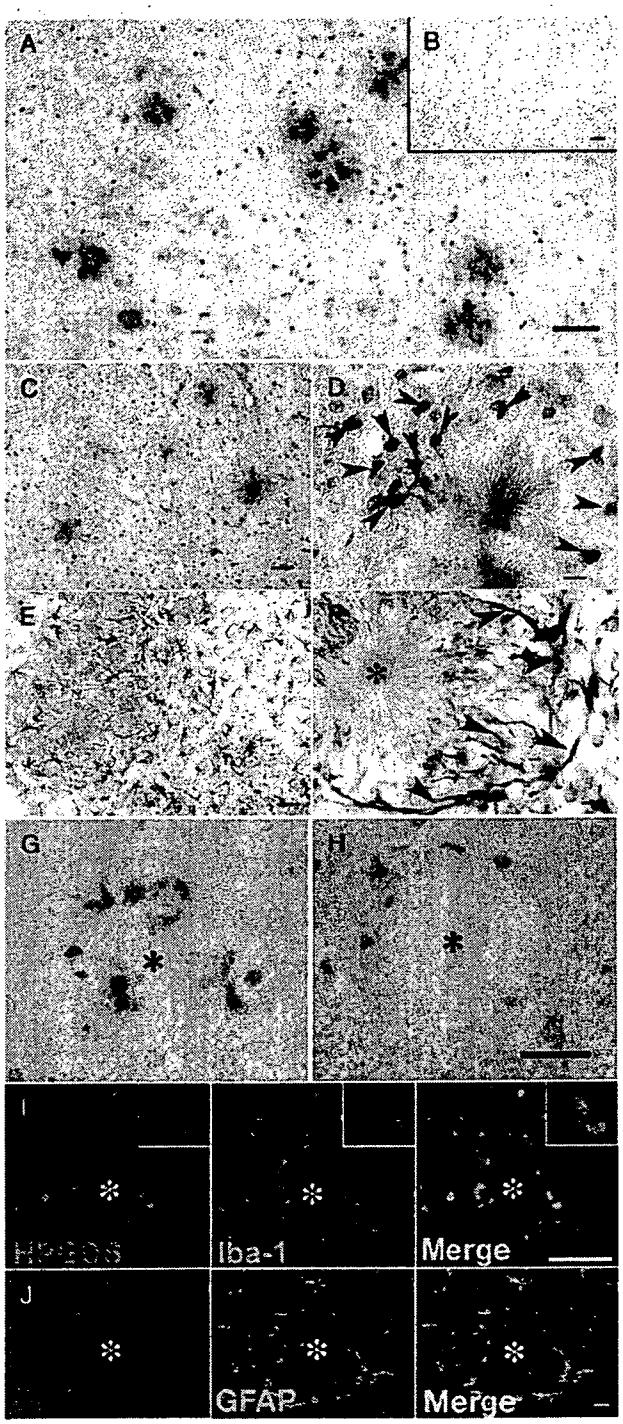

FIGURE 5. **(A, B)** Amyloid β (Aβ) immunostaining of primary motor cortex of Tg2576 **(A)** and wild-type **(B)** brains from 2-year-old mice. Scale bar = 200 μm. **(C, D)** Combination of Congo red staining (pink) and Iba1 immunocytochemistry (brown) in a Tg2576 mouse brain. **(D)** The arrowheads and asterisk indicate Iba1-positive activated microglia and an amyloid plaque, respectively. Scale bars = **(C)** 200 μm; **(D)** 20 μm. **(E, F)** Combination of Congo red staining (pink) and glial fibrillary acidic protein (GFAP) immunocytochemistry (brown) in a Tg2576 mouse brain. **(F)** Arrowheads and asterisk indicate processes of GFAP-positive astrocytes and an amyloid plaque, respectively. Scale bars = **(E)** 100 μm; **(F)** 20 μm. **(G, H)** Hematopoietic prostaglandin D synthase (HPGDS) immunocytochemistry on a Tg2576 mouse brain. HPGDS-positive cells surround a small reactive amyloid plaque **(G)** but not the large burned out class of plaques **(H)**. Asterisks indicate amyloid plaques. Scale bar = 20 μm. **(I)** Double immunofluorescence for HPGDS (pink) and Iba1 (green). Some of the Iba1-positive microglia express HPGDS. Scale bar = 50 μm. Inset shows a high magnification view of double-positive cells showing morphologic characteristics of ameboid microglia. **(J)** Double immunofluorescence for DP_1 (red) and GFAP (green). DP_1 is expressed on the processes of reactive astrocytes that have extended toward the center of this amyloid plaque. Scale bar = 10 μm.

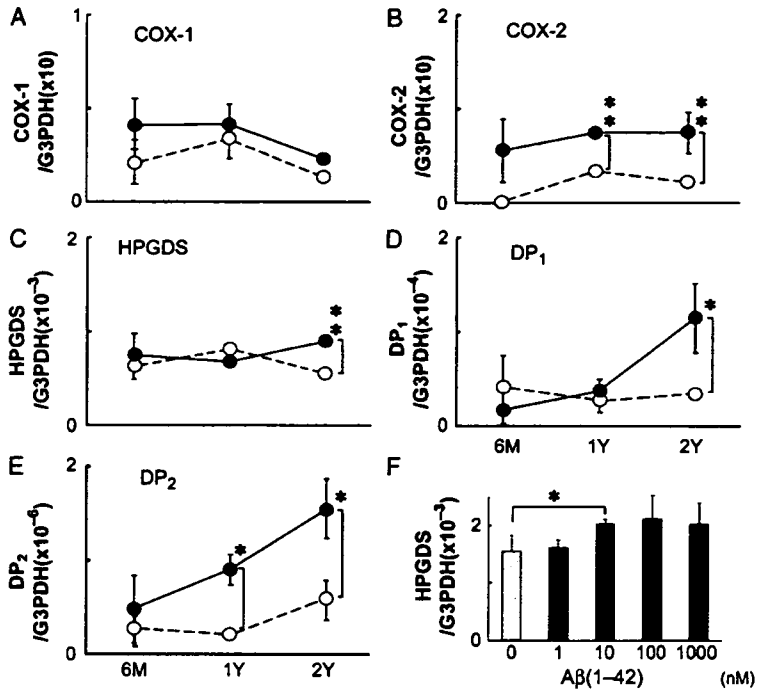

FIGURE 6. **(A–E)** Number of copies of mRNA for cyclooxygenase (COX)-1, COX-2, hematopoietic prostaglandin D synthase (HPGDS), DP_1, and DP_2 relative to that of glyceraldehyde-3-phosphate dehydrogenase (G3PDH) in brains from Tg2576 mouse (closed circles) and wild-type mouse (open circles) taken at the age of 6 months, 1 year, and 2 years (n = 3). *, $p < 0.05$; **, $p < 0.01$. **(F)** Number of copies of HPGDS mRNA relative to that of G3PDH from primary cultures of microglia before and after amyloid β (Aβ) (1-42) stimulation (n = 3) *, $p < 0.05$.

further increase was observed at concentrations higher than 10 nM (Fig. 6F).

DISCUSSION

HPGDS/PGD_2/DP_1 Signaling Pathway Plays Important Roles in Inflammatory Reactions Within the Senile Plaques

We demonstrated that expression of HPGDS and DP_1 was increased in reactive astrocytes and microglia encircling senile plaques in the AD brain. In contrast, the mRNA levels of all other prostanoid synthases and receptors were almost the same between AD and control groups. A previous study by Iwamoto et al (15) demonstrated that the amounts of PGD_2 and TXB_2 were significantly increased in the brains of Alzheimer-type dementia patients, although other prostaglandin metabolites in their AD group showed no significant changes from normal patients. In this study, we used a more specific and sensitive criterion for AD (9) and determined the levels of prostaglandin synthases and receptors instead of direct prostaglandin determination, because the latter is subject to a large postmortem artifact (16). In addition, we chose the most recent cases with the least postmortem interval for more accurate mRNA analysis. Ages and the postmortem interval of the patients at autopsy were not significantly different between AD and control groups.

Senile plaques have different characteristics depending on their stages (17); for example, there are primitive, neuritic (classic), and burned out class of plaques in various stage of human diseases. α-Macroglobulin and anti-chymotrypsin are expressed in the neuritic-type plaques but not in the burned out ones (18, 19). Although plaques homologous with neuritic plaques were not recognized in Tg2576 mouse brains, we observed that HPGDS expression was limited mainly to the relatively small plaques with surrounding activated microglia and was diminished in the burned out class of plaques in both human and mouse AD brains. These observations may explain why some patients did not show HPGDS mRNA upregulation and may suggest that HPGDS is responsible for early inflammation caused by Aβ accumulation in the evolution of amyloid plaques.

The question as to which is first, plaques or inflammation, still remains to be clarified. We previously demonstrated that secondary demyelination was suppressed by inhibition of PGD_2 production (8). We consider, therefore, that once the plaque is formed, microglia and astrocytes are activated and produce cytokines, which cause further neuronal injury and plaque formation. To clarify this, additional investigation is needed.

New Potential Therapies for Alzheimer Disease Based on Inhibition of the Hematopoietic Prostaglandin D Synthase/Prostaglandin D_2/DP_1 Signaling Pathway

Many epidemiologic and animal studies have revealed that nonsteroidal anti-inflammatory drugs (NSAIDs) are

beneficial for AD patients (20–24). For example, a large, prospective and population-based cohort study confirmed that the relative risk of developing AD was significantly reduced in long-term users of NSAIDs compared with nonusers (25). Furthermore, orally administered ibuprofen produced significant diminution of the ultimate number of amyloid deposits as well as significantly reduced gliosis in Tg2576 mice (24).

PGD_2 is formed from arachidonic acid, which is released from the lipid portion of membranes by $cPLA_2$, by successive enzyme reactions mediated by COX and PGD synthases. COXs, expression of which is upregulated in the AD brain (26, 27), are the major targets of NSAIDs. NSAIDs may reduce the plaque pathology through either their anti-inflammatory actions or suppression of γ-secretase activity (28, 29) or both. The latter reduces the level of the 42-amino acid form of Aβ protein (Aβ42), the most toxic form of the protein. NSAIDs inhibit the constitutively expressed COX-1 as well as the inducible COX-2, both of which produce PGH_2, a common precursor of PGD_2, PGE_2, $PGF_{2\alpha}$, prostacyclin (PGI_2), and TXA_2 (30). PGD_2 is well known as an inflammatory mediator: it augments vascular permeability (31), regulates chemotaxis (32) and antigen presentation (33), and inhibits platelet aggregation (34). The biologic actions of PGD_2 are elicited through binding to its receptors, DP_1 (35) or DP_2 (32). Regarding the anti-inflammatory property of NSAIDs, 3 molecular targets of these drugs have been identified so far in AD: COX-1, COX-2, and PPARγ. NSAIDs not only inhibit the activity of COXs but also activate the nuclear PPARγ (36), which inhibits the production of pro-inflammatory cytokines. All 3 of these NSAID targets seem to be expressed by activated microglia (5). In this study, the level of PPARγ was not changed in AD brains, although this finding does not exclude the possibility of PPARγ-mediated neuroprotection by NSAIDs.

COX-2 has been the major target of anti-inflammatory therapy and a previous study showed an approximately 25% increase in the COX-2 level in the frontal cortex of AD brains (n = 17) compared with that in control brains (n = 12), as determined by densitometric analysis of Northern blots (37). We detected upregulation of COX-2 mRNA in Tg2576 mouse brains but not in the 17 AD frontal cortices by quantitative RT-PCR analysis. Ueno et al (38) reported that HPGDS preferentially utilized COX-1 in the A23187-induced immediate response for PGD_2 synthesis. Therefore, which COX was upregulated along with HPGDS induction needs to be clarified. Although an inflammatory response can have either a potentially beneficial or detrimental outcome, the administration of an HPGDS inhibitor, HQL-79, to the twitcher mouse, which is an animal model of Krabbe disease, remarkably ameliorated their astrogliosis as well as their clinical symptoms (8). HPGDS inhibitors and DP_1 antagonists have already been developed as antiallergic drugs (39), and HQL-79 is an orally active inhibitor of HPGDS (40, 41) that can penetrate through the blood-brain barrier. These drugs will specifically inhibit the PGD_2 signaling pathway, whereas NSAIDs may inhibit the production of all prostanoids, including the neuroprotective PGE_2 (42, 43).

In conclusion, we propose that PGD_2 is a novel inflammatory mediator in the AD brain and that the efficacy of HPGDS inhibitors and DP_1 antagonists should be investigated for halting the devastating course of AD.

ACKNOWLEDGMENTS

We thank Dr. Shinichi Kousaka, National Center of Neurology and Psychiatry, Japan, for the generous gift of the anti-Iba1 antibody. We thank Ms. Shigeko Matsumoto for performing the immunocytochemical analysis and Ms. Megumi Yamaguchi, Ms. Megumi Yamada, and Ms. Taeko Nishimoto for their secretarial assistance.

REFERENCES

1. Selkoe DJ. Alzheimer's disease: Genes, proteins, and therapy. Physiol Rev 2001;81:741–66
2. Griffin WS, Stanley LC, Ling C, et al. Brain interleukin 1 and S-100 immunoreactivity are elevated in Down syndrome and Alzheimer disease. Proc Natl Acad Sci U S A 1989;86:7611–15
3. Rogers J, Luber-Narod J, Styren SD, et al. Expression of immune system-associated antigens by cells of the human central nervous system: Relationship to the pathology of Alzheimer's disease. Neurobiol Aging 1988;9:339–49
4. Pike CJ, Cummings BJ, Cotman CW. Early association of reactive astrocytes with senile plaques in Alzheimer's disease. Exp Neurol 1995; 132:172–79
5. Akiyama H, Barger S, Barnum S, et al. Inflammation and Alzheimer's disease. Neurobiol Aging 2000;21:383–421
6. Hsiao K, Chapman P, Nilsen S, et al. Correlative memory deficits, Aβ elevation, and amyloid plaques in transgenic mice. Science 1996;274: 99–102
7. Kawarabayashi T, Younkin LH, Saido TC, et al. Age-dependent changes in brain, CSF, and plasma amyloid (β) protein in the Tg2576 transgenic mouse model of Alzheimer's disease. J Neurosci 2001;21:372–81
8. Mohri I, Taniike M, Taniguchi H, et al. Prostaglandin D_2-mediated microglia/astrocyte interaction enhances astrogliosis and demyelination in twitcher. J Neurosci 2006;26:4383–93
9. Murayama S, Saitoh Y. Neuropathological diagnostic criteria for Alzheimer disease. Neuropathology 2004;24:254–60
10. Hughes CP, Berg L, Danziger WL, et al. A new clinical scale for the staging of dementia. Br J Psychiatry 1982;140:566–72
11. Lazarus M, Kubata BK, Eguchi N, et al. Biochemical characterization of mouse microsomal prostaglandin E synthase-1 and its colocalization with cyclooxygenase-2 in peritoneal macrophages. Arch Biochem Biophys 2002;397:336–41
12. Mohri I, Eguchi N, Suzuki K, et al. Hematopoietic prostaglandin D synthase is expressed in microglia in the developing postnatal mouse brain. Glia 2003;42:263–74
13. Forman BM, Tontonoz P, Chen J, et al. 15-Deoxy-δ 12,14-prostaglandin J_2 is a ligand for the adipocyte determination factor PPARγ. Cell 1995; 83:803–12
14. Kagitani-Shimono K, Mohri I, Oda H, et al. Lipocalin-type prostaglandin D synthase (β-trace) is upregulated in the αB-crystallin-positive oligodendrocytes and astrocytes in the chronic multiple sclerosis. Neuropathol Appl Neurobiol 2006;32:64–73
15. Iwamoto N, Kobayashi K, Kosaka K. The formation of prostaglandins in the postmortem cerebral cortex of Alzheimer-type dementia patients. J Neurol 1989;236:80–84
16. Narumiya S, Ogorochi T, Nakao K, et al. Prostaglandin D_2 in rat brain, spinal cord and pituitary: Basal level and regional distribution. Life Sci 1982;31:2093–2103
17. Probst A, Brunnschweiler H, Lautenschlager C, et al. A special type of senile plaque, possibly an initial stage. Acta Neuropathol (Berl) 1987; 74:133–41
18. Van Gool D, De Strooper B, Van Leuven F, et al. α_2-Macroglobulin expression in neuritic-type plaques in patients with Alzheimer's disease. Neurobiol Aging 1993;14:233–37